Vibration Interaction in a Multiple Flywheel System

THESIS

Jordan Firth, Captain, USAF

AFIT/GA/ENY/11-M03

DEPARTMENT OF THE AIR FORCE
AIR UNIVERSITY

AIR FORCE INSTITUTE OF TECHNOLOGY

Wright-Patterson Air Force Base, Ohio

AFIT/GA/ENY/11-M03

Vibration Interaction in a Multiple Flywheel System

THESIS

Presented to the Faculty

Department of Aeronautics and Astronautics

Graduate School of Engineering and Management

Air Force Institute of Technology

Air University

Air Education and Training Command

In Partial Fulfillment of the Requirements for the

Degree of Master of Science in Astronautical Engineering

Jordan Firth, B.S. Engineering Mechanics

Captain, USAF

March 2011

AFIT/GA/ENY/11-M03

Vibration Interaction in a Multiple Flywheel System

Jordan Firth, B.S. Engineering Mechanics
Captain, USAF

Approved:

Jonathan T. Black, Ph.D. (Chairman)	14 MAR 2011 Date
Richard G. Cobb, Ph.D. (Member)	14 MAR 2011 Date
Eric D. Swenson, Ph.D. (Member)	14 Mar 2011 Date

Abstract

This study uses a linear model of an Integrated Power and Attitude Control System (IPACS) to investigate the vibration interaction between multiple flywheels. An easily extendable MATLAB® script is created for the analysis of flywheel vibrations. This script is used to build a vibration model consisting of two active magnetic bearing flywheels mounted on a support structure. The flywheels are rotated at varying speeds, with an imbalance-induced centripetal force in one or both wheels causing vibrations in both wheels. Flywheel and system responses are examined for low frequency vibrations which would cause undesirable excitation to a satellite using IPACS, with a specific focus on the beat phenomenon and extra-synchronous vibration. Extra-synchronous resonant vibration between multiple rotors is shown to exist in an ideal undamped configuration but even a very small realistic amount of damping is enough to mitigate the effect enough that it is of less concern than individual rotor vibration inputs. Extra-synchronous resonant vibration is thus shown to have a minimal effect on satellite IPACS operation.

I Corinthians 10:31

Acknowledgements

Writing this thesis was more difficult than I had anticipated, and I could not have done it without significant help along the way. Dr. Black, thanks for your continual encouragement from beginning to end. Dr. Cobb and Dr. Swenson, thank you for saving *future* readers from a miry swamp of confusion. To my fellow late night Astro lab inhabitants, thanks for the energy.

And of course, many many thanks to my loving and incredible wife, who fed and took care of me during a grueling 5 months.

Jordan Firth

Table of Contents

Page

List of Figures

List of Tables

List of Acronyms

Acronym	
COM	center of mass
DOF	degree of freedom
EOM	equation of motion
IPACS	Integrated Power and Attitude Control System
ISS	International Space Station
MOI	moment of inertia
NASA	National Aeronautics and Space Administration
PSD	power spectral density
RPM	revolutions/minute
RPS	revolutions/second

Nomenclature

$\mathbf{0}$	appropriate size matrix of zeros
$\mathbf{A}$	state matrix
$\mathbf{B}$	input stiffness matrix
$\mathbf{C}$	damping matrix
$\mathbf{G}$	gyroscopic stiffness matrix
$\mathbf{I}$	appropriate size identity matrix
$\mathbf{K}$	spring stiffness matrix
$\mathbf{M}$	mass matrix
$\mathbf{R}$	rotation matrix
$\boldsymbol{a_c}$	centripetal acceleration
$\boldsymbol{e}$	flywheel eccentricity
$\boldsymbol{f_c}$	centripetal force
$\boldsymbol{q}$	state vector
$\boldsymbol{r}$	vector of displacement states
$\boldsymbol{\theta}$	vector of rotation states
$\boldsymbol{u}$	vector of input forces
c	translational damping
C	rotational damping
f_i	frequency of i$^{\text{th}}$ vibration mode, in Hz
I	moment of inertia
k	translational spring stiffness

m	body mass
P	rotor configuration (I_P/I_T)
t	time
x	$x-$axis
y	$y-$axis
z	$z-$axis
κ	rotational spring stiffness
ρ	radial distance between flywheel center of mass and shaft center
θ	axial flywheel rotation (short form of θ_z)
ξ	ratio of damping to stiffness
ω	wheel spin speed (short form of $\dot{\theta}_z$)

Subscripts

1	first flywheel or body
i	i$^{\text{th}}$ flywheel or body
i, j	between i$^{\text{th}}$ and j$^{\text{th}}$ bodies
n	n$^{\text{th}}$ flywheel or body
P	polar (about θ_x)
T	transverse (about θ_x and/or θ_y

Vibration Interaction in a Multiple Flywheel System

I. Introduction

Advanced flywheels are an exciting technology with the potential to greatly improve performance for satellite energy storage systems. They have been investigated for use in space since the early 1960's, and supporting technologies are finally beginning to mature to the point that they may soon be feasible. Unfortunately, despite much historic optimism, there are still unsolved and unstudied problems with their operation and implementation. This thesis investigates two areas of potential concern to see whether they pose any particular challenges to advanced flywheel operation in space: the beat phenomenon and extra-synchronous whirl excitation caused by interactions between multiple connected, unbalanced flywheels. This thesis also provides a flexible dynamics model of vibrations that can be used to study various Integrated Power and Attitude Control System (IPACS) configurations.

1.1 Definitions

For the purpose of this thesis, a *battery* will refer to a secondary electrochemical cell battery. A *flywheel* is a rotating mass which is used to store kinetic energy. An *advanced flywheel* will be a flywheel unit consisting of a high-speed, high-moment of inertia (MOI), low-mass rotor, frictionless electromagnetic bearings, a brushless electric motor/generator, and the electronics necessary to control the motor and bearings, as well as the associated support structure. In this thesis, advanced flywheels are assumed but not explicitly stated each time. Flywheels as studied here are those primarily intended for energy storage, which excludes similar reaction wheel and control moment gyro systems. A satellite flywheel energy storage system, usually referred

to in the context of an *IPACS*, contains a minimum of two flywheel units in order to allow for a net zero angular momentum and prevent uncontrolled spinning of the satellite. Four flywheel units are required for full, uncoupled, 3-axis attitude control and energy storage in a non-gimbaled configuration.

Whirl is a natural, resonant, rigid body, gyroscopic vibration mode in the form of a precession motion that occurs in a rotor/bearing system. It is described in Section 2.3.5. *Extra-synchronous* whirl excitation refers to two whirl modes at other-than-wheel speeds: *sub-synchronous*, which is below the speed of the rotor in question, and *super-synchronous*, which is above it. A spinning unbalanced rotor causes a vibration input at its own wheel speed (spin speed), but there are resonant vibration modes at frequencies other than the spin frequency. In a multiple flywheel system, a second rotor provides a direct source of vibration at extra-synchronous speeds.

1.2 Overview

All satellites have electronic equipment which requires electrical energy to run. Since power from solar cells is not available continuously, satellites need an energy storage subsystem. During periods of excess power generation, extra energy is stored in a battery. When the satellite needs more power than the solar cells can generate, it uses the energy stored in the battery. One alternative to chemical batteries for energy storage is advanced flywheels. Flywheels have not yet been used for energy storage in any space missions, but the technology is maturing quickly, and someday they may be a viable alternative for the satellite designer.

One additional benefit of flywheel-based energy storage is its inherent ability to control the attitude of a satellite. Many satellites use some form of momentum exchange device for attitude control. Since a flywheel system has multiple rotating wheels it can change the satellite's attitude by exchanging momentum between flywheels and

the spacecraft. Thus an IPACS, if well designed, can save weight by combining two necessary components of the satellite bus.

There are two key performance measures for a satellite energy storage system: high specific energy and high specific power. In addition, the energy storage system must meet several requirements in order to be considered for use in space. It must operate maintenance-free in widely-varying temperature conditions and survive in a radiation environment. It must perform under these conditions throughout a long lifetime—often greater than 10 years, with multiple daily charge/discharge cycles during its entire operational lifetime. It must survive a harsh vibration regime during launch, without itself creating unwanted vibration in the satellite during operation. Finally, it must be completely reliable from the beginning of the satellite's lifetime to the end.

Batteries, used for energy storage on every satellite, are far from ideal. They can provide either high specific power or high specific energy, but not both. They have a limited lifetime, measured not just from the beginning of their service life, but from the date of manufacture. They also require a carefully controlled thermal environment to avoid performance loss or even damage. They do excel in a few key areas, however. They are relatively simple and create zero external disturbances. Most importantly, the technology is mature and there is a long history of battery usage on satellites. They have proven to be predictable and reliable when used in a well-designed system.

Flywheel energy storage systems have not yet been used in any space system, but in some ways their theoretical performance is far better than that of batteries. A flywheel system is able to satisfy demands for high specific energy and power. It can theoretically do so without significant degradation for an extremely long life measured both in time and in charge/discharge cycles—lifetime is a minor design factor, but some current plans call for flywheels designed to operate for 15 years and 90 thousand

cycles. A flywheel system can operate in any thermal environment suitable for the satellite.

Unfortunately for the satellite designer, however, flywheel technology is far less mature than battery technology. Flywheel systems have not yet been developed at scales appropriate for satellites. Current systems exist only as bench-top research units, and the power supplies and drive electronics have not been scaled to an appropriately small size. Also, flywheel systems have not yet demonstrated the required reliability. Furthermore, rotating unbalanced rotors inherently create vibration which must be eliminated or at least mitigated to avoid affecting satellite operations negatively.

For attitude control, no direct comparison between batteries and flywheels can be made. Instead, flywheels can be compared to the entire battery and momentum exchange attitude control systems. Batteries are intended as energy storage devices only, and with no moving parts, they offer no attitude control. On the other hand, any advanced flywheel system is more than adequate to offer attitude control for a satellite in at least one dimension. Solving all of the other problems of creating a space-worthy high performance flywheel will ensure that the system is able to control the rotor momenta sufficiently to orient the spacecraft. Some minor concerns are a slight oversizing of the system—to ensure sufficient margin for both energy storage and attitude control—and appropriate geometry and control laws. The control laws for flywheel attitude control are non-trivial, but engineers have been developing them for decades and they currently await hardware implementation.

While there are still hurdles in the way of widespread flywheel system adoption on satellites, an incredible array of challenges have already been solved. High tensile strength carbon fibers enable the creation of light and strong rotors. Actively controlled contact-free magnetic bearings waste no energy as heat due to friction,

with minor and controllable system losses in other areas. Advanced brushless motor/ generators allow for very efficient energy storage. Good design and robust computer control of the bearings and motors enables stability throughout the operating regime. Two problems that remain are scaling the technology to a reasonable size and ensuring an acceptable level of system vibration.

After solving all technical problems satisfactorily, there are two remaining steps to be completed before widespread adoption of advanced flywheels is possible. First, a reasonably sized, operationally representative unit needs to be built and tested. To date, most work has been performed on either larger systems or component-wise on smaller parts. A reasonably sized unit would include all necessary components in a package small enough to fit in a simple technology demonstrator. Finally, a successful technology demonstration satellite must be flown to give other satellite designers proof that flywheels are viable in space.

1.3 Objectives

This thesis will examine the problem of flywheel-induced vibrations on satellites, focusing on the interactions between multiple imperfect flywheels at varying speeds and the vibration inputs this imbalance creates for a satellite. Even the most precisely manufactured flywheels have some residual imbalance. At wheel speeds of high tens of thousands of revolutions/minute (RPM), this vibration creates a potentially harmful amount of vibration. Bearings and soft mounts reduce this vibration, but they cannot completely eliminate it.

In addition to the individual flywheels, the entire IPACS consisting of multiple flywheels must keep vibration within an acceptable limit. The envelope must include the interaction of multiple wheels operating at different combinations of speeds. Previous flywheel vibration research has focused primarily in single-rotor vibration rather

than vibration interaction. This thesis will develop a linear state-space model to investigate potential sources of low frequency system excitation caused by beat phenomena and extra-synchronous whirl excitation as two connected flywheels operate as part of an IPACS. A linear model is sufficient to prove the existence of gyroscopic vibration interaction. The model will be used to study a two-flywheel system. However, the model is flexible enough to be used in future investigations of IPACS with an arbitrary number of individually oriented flywheels.

This thesis will seek to answer the question of whether the beat frequencies caused by similar flywheel rotation speeds or the extra-synchronous interactions between multiple connected flywheels can cause harmful low frequency vibration in an IPACS. Results will be limited by the model assumptions: fixed-satellite, small angle rotations, linear springs, and limited geometry and input configurations. These assumptions are described in Section 2.5.

1.4 Organization

This thesis is organized as follows: Chapter I provides a brief overview of the thesis. Chapter II reviews relevant literature on the subject of flywheels and provides background information in support of the thesis. The modeling methodology and validation are covered in Chapter III. Chapter IV details the results of the analysis, and Chapter V summarizes the conclusions and recommendations.

II. Background

2.1 Literature Review

A flywheel is a device that stores rotational kinetic energy for later use in the form of a rotating mass. Flywheels have countless applications, both realized and theoretical, but one as yet unrealized application is the use of flywheels onboard a satellite for energy storage. A flywheel system—at least two wheels would be necessary—could supplement or even replace the secondary cell electrochemical batteries on the satellite. In addition, with appropriate control algorithms, the flywheel system could be used to provide both energy storage and attitude control to the satellite. IPACS offers potential performance benefits and weight savings (and consequently cost savings) to the satellite designer. Flywheels have practical potential applications on the ground as well as in space, but this review will be primarily limited to space applications.

As described by Genta, flywheels have been used for millenia, from the invention of spindles and potter's wheels. The high inertia of a rotating flywheel smooths out changes in the motion of a rotating body. Motors often rely on this smoothing for steady output, and many types of motor would not operate at all without a flywheel (5:3,16).

Flywheels have a long engineering heritage, but Sputnik was only launched in 1957, so the problem of energy storage in space is just over 50 years old. A flywheel energy storage system for satellites was first proposed by Roes only a few years later (7:17–18).

No IPACS paper would be complete without a reference to Roes. In 1961, he proposed a flywheel system for satellite energy storage (7:8). He did not consider using flywheels for attitude control, only for energy storage. The idea of combining the attitude control and energy storage functions of a flywheel into an IPACS began to

appear in the early 1970's in several technical papers from the National Aeronautics and Space Administration (NASA) Langley Resarch Center (7:17–18).

Early flywheel studies were not limited to the investigation of advanced flywheels. In a 1997 report, Hall states that, "several studies in the 1960's and 1970's indicated that the use of steel flywheels on mechanical bearings would be competitive with the chemical batteries of the time (7:5)."

Since then, flywheels have been continually studied for space applications. NASA commissioned the enormously detailed *Integrated Power/Attitude Control System (IPACS) Study* in 1974 and a similarly thorough *Advanced Integrated Power and Attitude Control System (IPACS) Study* in 1985. Contemporary theoretical system performance has continued to climb, but not at the rate anticipated by some designers. Practical system performance by necessity lags even further behind. In 1976 NASA predicted a system energy density of 300 W-hr/kg by the year 2000. By 1992, this prediction was lowered to 100 W-hr/kg with a statement that not all failure modes or safety needs had yet been identified for such systems (7:10).

Progress has been made in a variety of areas since then, however. Among these advances in theory and application are high efficiency electric motors, magnetic bearings, composite rotors, and advanced attitude control algorithms. In 1985, Genta published the seminal *Kinetic Energy Storage*, which was an attempt to summarize flywheel engineering efforts for all applications and provide an up to date review of the subject (5:v).

While much advanced flywheel technology has been developed for aerospace applications, the benefits are beginning to spread to other industries. By 1996 advanced flywheels were beginning to be considered for use in several terrestrial applications, including uninterruptible power supplies and hybrid vehicles (20). The U.S. Navy is currently using flywheels and associated technology in development and fielding of

their Electromagnetic Aircraft Launch System to replace steam catapults on aircraft carriers (3).

Active magnetic bearings are a critical enabling technology for advanced flywheels. In a vacuum they are frictionless, reducing or eliminating many of the problems otherwise associated with bearings for such high speed devices. The controllable bearing stiffness can be low, isolating the inherent vibrations caused by an unbalanced rotor. In addition, filters and other control algorithms can be used to control the bearings such that the the vibration isolation is tuned to problem areas (15:2).

At the turn of the century, flight prospects for flywheels looked great. NASA had been working with with U.S. Flywheel Systems, Inc., TRW, Texas A&M University, the University of Texas, and Boeing for five years to develop and build advanced flywheels. These efforts were rewarded in December of 1999 with a successful test run of their D1 flywheel unit at 60,000 RPM—a then-world record for a magnetic bearing flywheel. These efforts were intended to lead to a technology demonstration payload for the International Space Station (ISS).

By 2001, plans were firmly in place for the most promising space-based technology demonstration to date. NASA had continued to work on plans for a technology demonstration, and onboard testing of a Flywheel Energy Storage System for the ISS was to begin by 2005. A successful test of the system could have led to the eventual replacement of the station's batteries (14:2). Unfortunately, funding for this program was cancelled in 2002 (2), and no further solid plans for a technology demonstration have been made.

Some residual flywheel development continued, however. In July of 2003, NASA demonstrated a basic IPACS capability on an air bearing table with two flywheel modules (19:64). The test setup can be seen in Figure 1. Meanwhile, NASA was working on the more advanced G2 flywheel module with better performance. This

was the first flywheel module designed in-house by NASA's Glenn Research Center. It had a higher power rating, lower spin losses, and a more generous thermal envelope than the previous D1 flywheel.

Figure 1: Photo of NASA's D1 and HSS flywheels demonstrating integrated power and attitude control, July 2003 (19:64)

In September of 2004, NASA successfully tested the G2 flywheel module to a speed of 41,000 RPM. G2 is shown in Figure 2 (9:132). Later that month, the same team placed two flywheel modules (the older D1 and the newer G2) on an air bearing table to demonstrate a full IPACS capability. They succeeded in demonstrating controllable torque up to ± 0.8 N-m and power transfer from 0–300 W. This was a first for high-power, high-speed IPACS. Since then, however, active efforts towards a flight-worthy technology demonstration have remained stalled.

With more recent technology advances, some researchers are beginning to design small IPACS for small satellites with demanding mission profiles. Lappas et al. discussed this in an article that appears to be the most recent comprehensive review of IPACS history and literature (12).

The control algorithms for IPACS have been studied very thoroughly, with many papers written about both energy/power storage and attitude control. Two types of

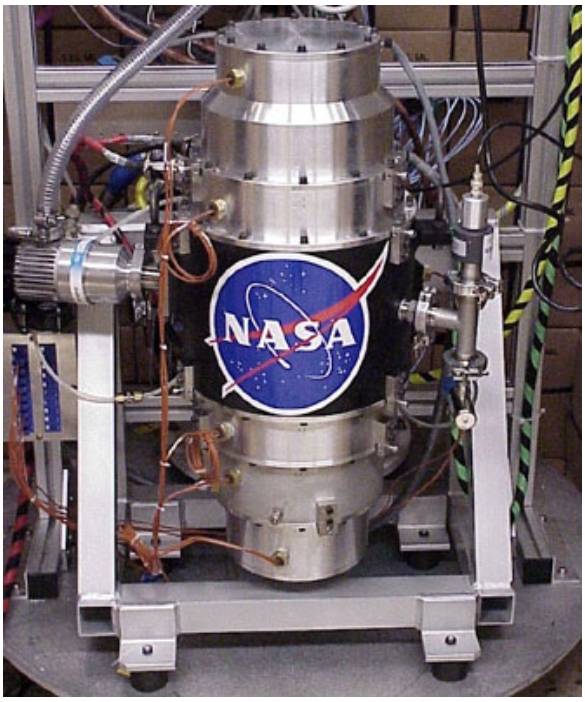

Figure 2: Photo of NASA's G2 flywheel module, tested to 41 kRPM in 2004 (10:95)

attitude control models have been studied: gimbaled CMG-like flywheels and fixed momentum wheel-like flywheels (7:22). Hall demonstrated that with the minimal momentum wheel configuration (4 flywheels), the attitude control and energy storage functions of an IPACS system could be completely decoupled. This simplifies control development for both functions (6:1894).

To date, the study of IPACS vibrations has been very limited. Previous IPACS research has focused heavily on control algorithms, assuming rigid bearings and perfectly balanced flywheels. In his Ph.D. dissertation, Park studied an IPACS with flexible magnetic bearings, unbalanced flywheels, and flexible appendages. He used the imbalances and appendages as inputs to an IPACS to develop control algorithms and physical means to mitigate problems in an IPACS. He found that wheel-speed notch filters in the control algorithm and vibration control masses on the end of flexible satellite components could effectively reduce vibration and power surge problems in the IPACS and consequently in the satellite (15). Park's physical model was similar

to the one developed in this thesis, but this thesis investigates instead the interactions of vibrations between multiple flywheels.

The beat frequency has been studied briefly in rotordynamics. Research performed at the Naval Postgraduate School used the beat frequency as a tuning aid to match filter frequencies to vibration frequencies (13). The equations of motion for a rigid body gyroscope are linear, however, and since the beat frequency's effects on a linear system are small as shown in Section 2.3.6, there has not been much study of the effects of beat frequency in flywheel systems. One exception is a NASA investigation on beat frequency effects caused by pulse width modulation of position sensor signals for a magnetically suspended flywheel rotor, but this model dealt with non-linear effects rather than linear physical behavior (11).

While IPACS vibration has been largely neglected, the study of a single flywheel's vibration is completely within the realm of rotordynamics, which is very well studied and is applicable to a wide variety of modern mechanical systems. Vance's *Rotordynamics of Turbomachinery* is one of the early comprehensive books on the subject (22:iv). Research in the field of rotordynamics is ongoing, and with the advent of realizable controlled magnetic bearings, the state of the art continues to advance.

IPACS research has been ongoing for 50 years now, and no immediate demonstration is planned. The main obstacle in the way of a successful flight demonstration is the complexity the problem—using an advanced and dynamic system to perform two unrelated tasks. While many of these complications have been studied and some of them have been mitigated, the vibration interactions between multiple flywheels in one IPACS have been neglected. This thesis seeks to provide a look into the problem of vibration interaction in order to determine whether it will be a problem for IPACS in space. To peform this study, a flexible dynamics model is developed that will enable research into vibrations of multiple gyroscope systems.

2.2 Coordinates and Nomenclature

There are two types of coordinates used in this model: wheel-aligned and global. Both coordinate frames are right-handed in x, y, and z, with corresponding rotations θ_x, θ_y, and θ_z.

The wheel-aligned coordinates are oriented such that the z axis is along the flywheel spin axis for the wheel in question. The spin axis always points away from the support structure, which is the system center of mass (COM). The x and y axes are arbitrary in this coordinate frame since all inputs and outputs are cyclical in nature about z. All discussions of individual flywheels refer to these local coordinates, including all imbalance-induced input forces and wheel speeds.

The global coordinates are arranged with z "up". This coordinate frame is arbitrarily aligned. All system level references—including all response plots shown in this thesis—will use the global coordinate system. Model inputs are applied internally in the global frame. Coordinate systems are arranged as shown in Figure 3.

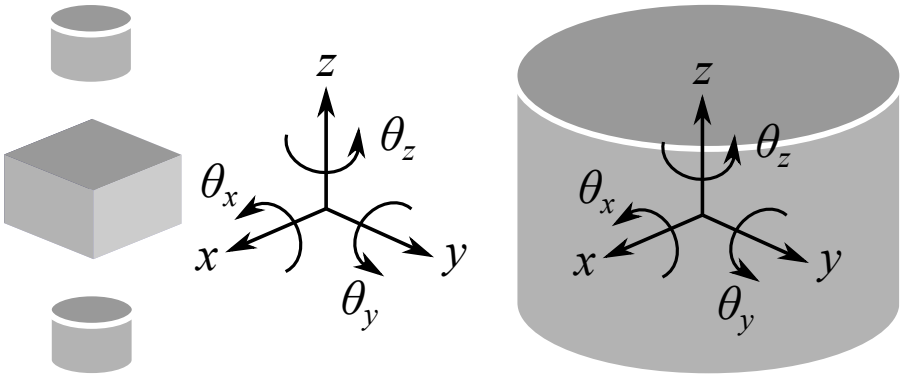

(a) Global Coordinates (b) Wheel-aligned Coordinates

Figure 3: Coordinate systems used in this thesis

Nomenclature is defined as it is introduced, as well as appearing in a nomenclature section at the beginning of this thesis. A few terms are potentially confusing, so a preview of them is in order here. Rotation angles $\theta_{x,y,z}$ are defined as shown in

Figure 3. $\boldsymbol{\theta}$ is the vector of rotational states $\left(\begin{bmatrix}\theta_x & \theta_y & \theta_z\end{bmatrix}^{\mathrm{T}}\right)$, which are rotations about x, y, and z, respectively. In the discussion of flywheels and rotors, wheel rotation and speed are of particular importance, so θ with no letter subscript will refer to the rotation angle of a rotor. Similarly, ω with no letter subscript will refer to rotor speed, which would otherwise be referred to as $\dot{\theta}_z$.

Furthermore, there are three sets of units in widespread use to describe rotational speed: rad/s, RPM, and Hz or revolutions/second (RPS). Flywheel dynamics must be calculated in radians, but discussion is more intuitive in units of Hz or RPS. Finally, system-level discussions of high-speed advanced flywheels commonly uses units of RPM. The model developed in this thesis uses units of radians and rad/s internally, but most discussion of wheel speeds in this paper will be in terms of Hz and RPS.

2.3 Fundamental Equations

Understanding of several basic sets of equations is required for the study of flywheel motion. A quick overview of some of these concepts is provided here.

2.3.1 Equation of Motion for a Gyroscopic Body. In this model, flywheels are modeled as gyroscopic rigid bodies. The equation of motion (EOM) for a gyroscopic rigid body is shown in matrix form in Equation 1 (18:124). Equation 1 also describes the equation of motion for a non-spinning rigid body since gyroscopic stiffness, $\mathbf{G}$, is a function of wheel speed, ω, and it is zero for a non-spinning body.

$$\mathbf{M}\ddot{\boldsymbol{q}}(t) + \left(\mathbf{C} + \mathbf{G}\left(\omega(t)\right)\right)\dot{\boldsymbol{q}}(t) + \mathbf{K}\boldsymbol{q}(t) = \boldsymbol{u}(t) \tag{1}$$

where the state vector $\boldsymbol{q} = \begin{bmatrix} \boldsymbol{r}^{\mathrm{T}} & \boldsymbol{\theta}^{\mathrm{T}} \end{bmatrix}^{\mathrm{T}}$ is composed of $\boldsymbol{r} = [x \quad y \quad z]^{\mathrm{T}}$ and $\boldsymbol{\theta} = [\theta_x \quad \theta_y \quad \theta_z]^{\mathrm{T}}$, $\boldsymbol{u}$ is a vector of input forces, $\mathbf{M}$ is the mass matrix described in terms of body mass m and directional MOI $I_{x,y,z}$. If the body is represented as a point mass, $\mathbf{M}$ is the diagonal matrix $\mathbf{M} = \mathrm{diag}\left(\begin{bmatrix} m & m & m & I_x & I_y & I_z \end{bmatrix}\right)$. $\mathbf{K}$ and $\mathbf{C}$ are the stiffness and damping matrices between the body and external nodes, and, when described in wheel-aligned coordinates, $\mathbf{G}$ is the sparse skew-symmetric gyroscopic matrix shown below.

$$\mathbf{G} = \begin{bmatrix} \ddots & & \vdots & \\ & 0 & -I_z\omega & 0 \\ \dots & I_z\omega & 0 & 0 \\ & 0 & 0 & 0 \end{bmatrix}.$$

In the simple case of a single body connected by springs to a fixed support, stiffness would be written as $\mathbf{K} = -\mathrm{diag}\left(\begin{bmatrix} k_x & k_y & k_z & \kappa_{\theta_x} & \kappa_{\theta_y} & \kappa_{\theta_z} \end{bmatrix}\right)$ with translational and rotational stiffnesses k and κ, respectively. Likewise, damping of a single body would be described by $\mathbf{C} = -\mathrm{diag}\left(\begin{bmatrix} c_x & c_y & c_z & C_{\theta_x} & C_{\theta_y} & C_{\theta_z} \end{bmatrix}\right)$ with translational and rotational damping of c and C.

In this model, however, the bodies will be connected not to fixed supports, but to each other. Proper modeling of this inter-body stiffness requires the use of different (and more complicated) stiffness and damping terms. These inter-body stiffness and damping terms are only applicable to a system rather than to individual rigid bodies, and they will be discussed in Section 3.3.1.

2.3.2 State-Space Equation of Motion. State-space representation is a convenient format for writing and solving linear differential equations, and it is the form that will be used for the model in this thesis. In general, a linear system can be

described in state-space according to Equation 2 (17:210). Note that the notational dependence on time is dropped for convenience.

$$\dot{\boldsymbol{q}} = \mathbf{A}\boldsymbol{q} + \mathbf{B}\boldsymbol{u} \tag{2}$$

where $\mathbf{A}$ is the state matrix that describes system behavior and $\mathbf{B}$ is an input matrix linking input forces to states.

Equation 3 below shows Equation 1, the gyroscopic EOM, in state-space form with the addition of an input matrix, $\mathbf{B}$. Note that the entire matrix EOM is found in the second half of this equation; the top half is simply a computational convenience.

$$\begin{bmatrix} \dot{\boldsymbol{q}} \\ \ddot{\boldsymbol{q}} \end{bmatrix} = \begin{bmatrix} \mathbf{0} & \mathbf{I} \\ \mathbf{M^{-1}K} & \mathbf{M^{-1}(C+G)} \end{bmatrix} \begin{bmatrix} \boldsymbol{q} \\ \dot{\boldsymbol{q}} \end{bmatrix} + \begin{bmatrix} \mathbf{0} \\ \mathbf{M^{-1}B} \end{bmatrix} \boldsymbol{u} \tag{3}$$

2.3.3 Rotated Equation of Motion. If the flywheel EOM is known in the wheel-aligned coordinate frame, but the integration is to be carried out in a different global coordinate frame, Equation 3 must be rotated accordingly. Recalling that the entire matrix EOM is found in the second half of the state-space equation, the correct application of the rotation matrix $\mathbf{R}$ is shown below in Equation 4. Proper rotation is required when a collection of bodies with different local coordinate frames is integrated into one state-space system.

$$\begin{bmatrix} \dot{\boldsymbol{q}} \\ \ddot{\boldsymbol{q}} \end{bmatrix} = \begin{bmatrix} \mathbf{I} & \mathbf{0} \\ \mathbf{0} & \mathbf{R} \end{bmatrix} \begin{bmatrix} \mathbf{0} & \mathbf{I} \\ \mathbf{M^{-1}K} & \mathbf{M^{-1}(C+G)} \end{bmatrix} \begin{bmatrix} \mathbf{I} & \mathbf{0} \\ \mathbf{0} & \mathbf{R^T} \end{bmatrix} \begin{bmatrix} \boldsymbol{q} \\ \dot{\boldsymbol{q}} \end{bmatrix} + \begin{bmatrix} \mathbf{0} \\ \mathbf{RM^{-1}BR^T} \end{bmatrix} \boldsymbol{u} \tag{4}$$

2.3.4 Centripetal Force. The primary input in this model will be the vibration caused by an unbalanced spinning flywheel rotor, which is a centripetal force. Equations 5 and 6 show the equations for centripetal acceleration, $\boldsymbol{a_c}$, and its associated force, $\boldsymbol{f_c}$ in polar coordinates (1:75–76).

$$\boldsymbol{a_c} = -\boldsymbol{\rho}\omega^2 \tag{5}$$

$$\boldsymbol{f_c} = -\boldsymbol{e}\omega^2 = -m\boldsymbol{\rho}\omega^2 \tag{6}$$

where eccentricity e represents rotor mass m and the distance between the flywheel's COM and the center of the shaft, ρ. Wheel speed is again represented by ω. The distance ρ is shown in Figure 4. The vectors $\boldsymbol{e}$ and $\boldsymbol{\rho}$ point from the center of mass to the flywheel shaft.

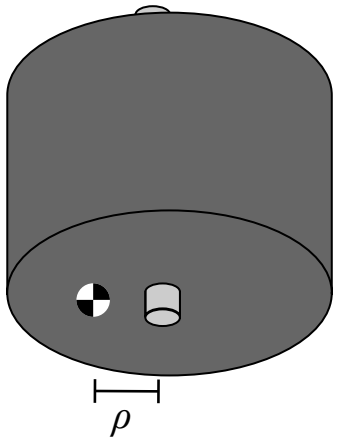

Figure 4: A spinning flywheel of mass m with COM–shaft distance ρ creates a centripetal input force proportional to eccentricity $e = m\rho$

2.3.5 Natural Frequencies of a Rotor/Bearing System. The IPACS model in this thesis will be used to evaluate vibration interactions. One potentially troublesome vibration is resonant frequency excitation of the flywheels. Rigid rotors have several

vibration modes, and those are briefly explained here. In this brief discussion of natural frequencies, ω_1–ω_4 will refer to natural frequencies of the rotor/bearing system, and ω with no subscripts will refer to wheel speed.

When a rigid rotor is restrained in the x and y directions by springs of stiffness K as shown in Figure 5, the EOM from Equation 1 can be simplified to the forms shown below in Equations 7–10.

$$m\ddot{x} + 2kx = 0 \tag{7}$$

$$m\ddot{y} + 2ky = 0 \tag{8}$$

$$I_T\ddot{\theta_x} + I_P\omega\dot{\theta_y} + \frac{1}{2}kL^2\theta_x = 0 \tag{9}$$

$$I_T\ddot{\theta_y} - I_P\omega\dot{\theta_x} + \frac{1}{2}kL^2\theta_y = 0 \tag{10}$$

where m = rotor mass, L = rotor length, and I_t and I_p are the transverse and polar MOIs, respectively (22:125).

The natural frequencies, ω_n, of the rigid body rotor/bearing system shown in Figure 5 and described in Equations 7–10 are shown in Equations 11–13. Recall that ω represents angular rotor speed.

$$\omega_1 = \omega_2 = \sqrt{\frac{2K}{m}} \tag{11}$$

$$\omega_3(\omega) = \frac{I_P}{2I_T}\omega + \sqrt{\frac{KL^2}{2I_T} + \left(\frac{I_P}{2I_T}\omega\right)^2} \tag{12}$$

$$\omega_4(\omega) = \frac{I_P}{2I_T}\omega - \sqrt{\frac{KL^2}{2I_T} + \left(\frac{I_P}{2I_T}\omega\right)^2} \tag{13}$$

Natural frequencies ω_1 and ω_2 correspond to translational vibration modes in the x and y directions. Frequencies ω_3 and ω_4 correspond to the forward and backward

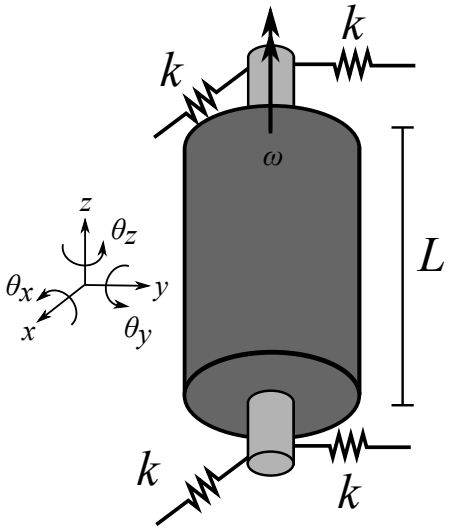

Figure 5: A long rigid rotor constrained by springs in x and y

whirling modes, respectively. Whirling is a precession-like motion. Forward whirl (ω_3) is rotation in the same direction as wheel spin, as shown in Figure 6. Backward whirl (ω_4) is rotation in the opposite direction.

Modes 1 and 2 are constant and identical. They represent "bouncing" in the x and y directions. There is no angular motion associated with these modes. The frequency of these modes is solely a function of bearing stiffness and rotor mass.

Modes 3 and 4 are, respectively, the speed-dependent forward and backward conical whirling motions. With a wheel speed of zero, $\omega_3(0) = \omega_4(0) = \omega_T = \sqrt{\frac{KL^2}{2I_T}}$, which is the natural rigid body pitching/yawing frequency. Rigid body vibration at this frequency will be simple pitching or yawing about θ_x or θ_y.

As rotor speed, ω, increases, the pitching and yawing motions become whirling motions, and the frequencies of the forward and backward whirls diverge from ω_T, with forward whirl speed increasing and backward whirl speed decreaseing. As wheel speed approaches infinity, ω_3 approaches P and ω_4 approaches 0. P is the ratio I_P/I_T (polar

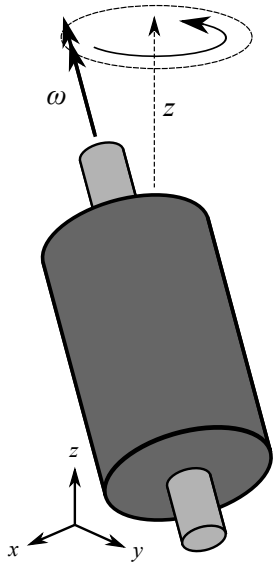

Figure 6: Depiction of forward whirling motion

MOI/transverse MOI), which represents rotor configuration. For a short coin-like disc or hoop, $P = 2$. For an infinitely long rotor, $P = 0$ (22:126).

Figure 7 shows the normalized natural frequencies of the forward and backward whirl modes, respectively. Recall that ω_T, the natural rigid body pitching/yawing frequency is $\sqrt{\frac{KL^2}{2I_T}}$. Backward whirl has a negative frequency value because it is in the direction opposite wheel spin. These modes are dependent on P, the rotor configuration (22:127).

Of the whirl modes, ω_3 is the mode most easily excited by rotor imbalance. Figure 7(a) shows that short rotors are not self-exciting for forward whirl, but long rotors have a critical coning frequency where the wheel frequency is synchronous with the whirl frequency. The critical coning frequency, ω_{con} is found by setting $\omega \equiv \omega_3$ in Equation 12, resulting in Equation 14.

$$\omega_{con} = \sqrt{\frac{\omega_T^2}{1 - P}} \tag{14}$$

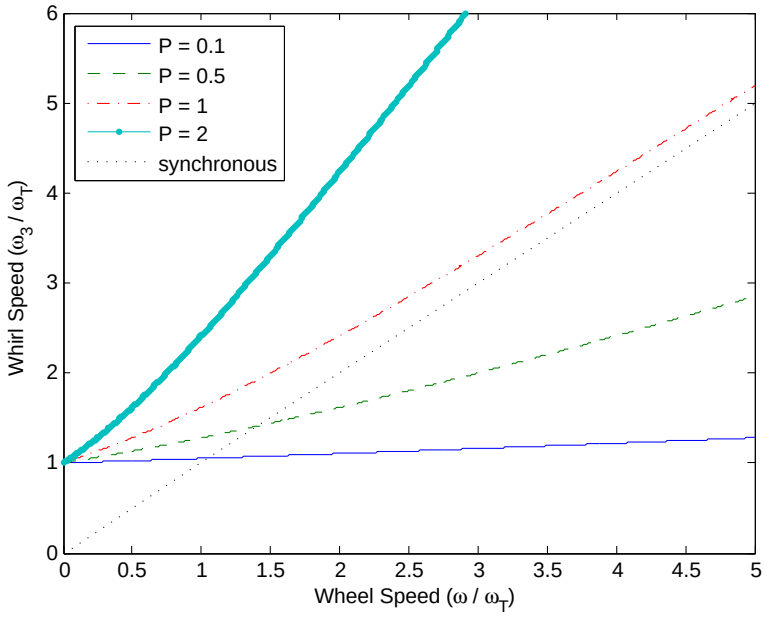

(a) Forward Whirl (ω_3)

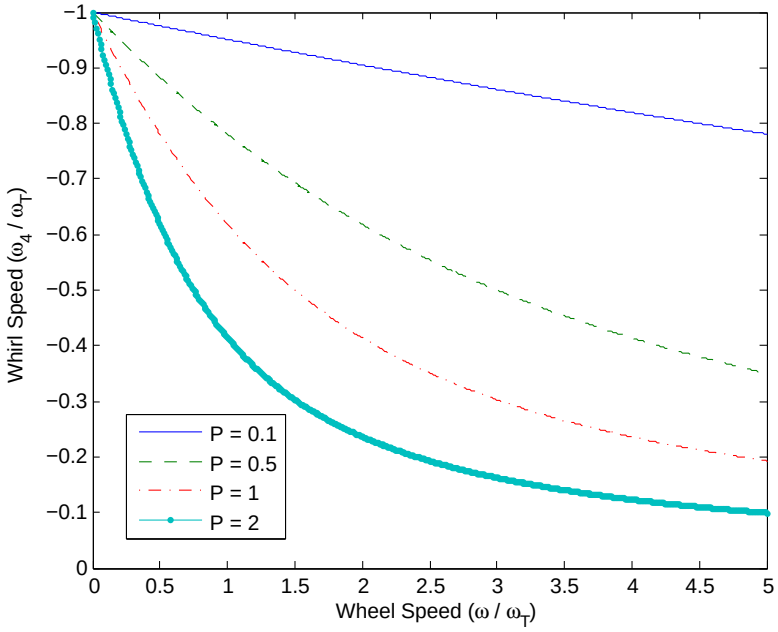

(b) Backward Whirl (ω_4)

Figure 7: Normalized whirl modes for various flywheel rotor configurations. Dotted line for forward whirl shows where whirl speed is synchronous with wheel speed. Natural rigid-body pitching frequency ω_T is used to normalize plots for all rotor/bearing configurations (22:128)

Operation near the critical coning frequency can be unstable, although momentarily passing through this region is acceptable, allowing operation in supercritical regions (21:354). For long rotors ($P < 1$), this critical frequency must be kept low enough to be out of the operating range of the rotor. Shorter rotors ($P > 1$) do not have this problem, but an outside excitation at the coning frequency could be hazardous. Outside excitation at critical coning frequencies is examined in this paper for both short and long rotors, which are the sub- and super-synchronous rotor frequency problems.

Natural frequencies ω_n as found in Equations 11–13 are described in units of rad/s. For the remainder of this thesis, natural frequencies will be instead described in units of Hz as f_n, where

$$f_n = \frac{\omega_n}{2\pi} \tag{15}$$

This terminology will eliminate any confusion between wheel speeds (described as ω) and the natural frequencies.

2.3.6 Beat Frequency. For linear systems, the response of a system to two inputs can be found by adding the system's response to the individual inputs. This superposition can yield a stronger or weaker response than either signal individually, depending on whether the sum of the responses is positive or negative, creating either constructive or destructive interference.

When waveforms of two frequencies (ω_1, ω_2) differ in frequency by a small amount δ, ($\omega_2 = \omega_1 + \delta$), the wave which results from their combination will exhibit what is known as a beat phenomenon due to alternating constructive and destructive

interference. Using the relationship

$$\sin A + \sin B = 2 \sin \frac{A+B}{2} \cos \frac{A-Y}{2},$$

the sum $(y_1 + y_2)$ of two displacements

$$y_1 = \sin \omega_1 t$$
$$y_2 = \sin \omega_2 t = \sin (\omega_1 + \delta) t$$

can be written as shown in Equation 16 (16:23).

$$y = y_1 + y_2 = 2 \sin \left(\omega_1 + \frac{\delta}{2} \right) t \cos \left(\frac{\delta}{2} \right) t \tag{16}$$

Figure 8 shows an example of a beat frequency created by the superposition of two waves with similar frequencies. The resultant waveform is a sine wave of frequency $\omega = \frac{\omega_1 + \omega_2}{2}$ which is shaped by the envelope described by $\pm 2 \cos \left(\frac{\delta}{2} \right) t$. This envelope has a much lower frequency than either of the original waves.

When two signals are combined in a linear system they are superimposed additively. In order to see system excitation at the beat frequency, there would have to be some non-linear process allowing the input frequencies to be multiplied. Otherwise, there will be no change in frequency. This lack of excitation at the beat frequency should manifest itself in a lack of energy at the beat frequency in a power spectral density (PSD) plot. The signal shown in Figure 8 was analyzed with the MATLAB® `pwelch` command to create the PSD plot shown in Figure 9.

As expected, Figure 9 shows that the signal in Figure 8 has energy at both input frequencies, but there is no system energy at the beat frequency of 5 Hz. In linear

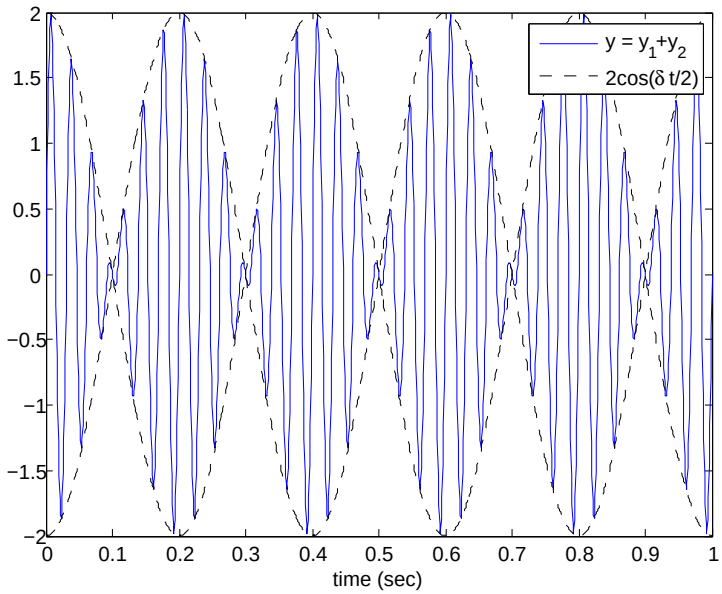

Figure 8: Beat phenomenon created by inputs of frequency 30 and 35 Hz

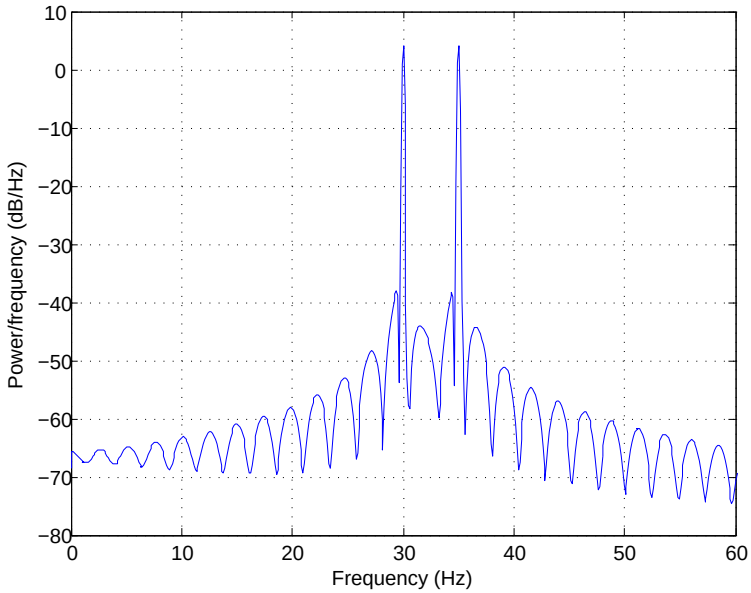

Figure 9: Power spectral density plot of the signal shown in Figure 8. Note the lack of energy at the beat frequency of 5 Hz

systems there should be no excitation at this beat frequency, even if some connected structure has a natural frequency close to the beat frequency.

2.4 Model

The model used in this thesis represents two advanced flywheels mounted to a support structure and nominally spinning in opposite directions. The rotors are mounted with active magnetic bearings, and their operating speed range is 20,000–60,000 RPM (333–1000 RPS). They are powered by high-efficiency motor/generators. The rotors nominally spin at the same speed to store energy, changing speed relative to each other to control the attitude of the satellite.

2.5 Scope

The model developed in this thesis relies on several assumptions to limit the scope of the analysis. The only source of vibration studied is rotor imbalance. There are multiple other real sources of vibration including torque ripple, sensor error, bandwidth limitations, and external vibrations. These additional vibration sources are ignored.

Also, this model does not take into consideration any motion of the satellite. In a satellite with an IPACS, the satellite body will be free to rotate, and can be controlled by the varying rotation rates of the flywheels. In the model used in this thesis, the IPACS is subjected mainly to symmetric or periodic disturbing forces from a static equilibrium state, and it does not experience large rotations. When necessary, a spring is used to enforce small angles. The spring constraint makes the use of small angle approximations for IPACS rotation appropriate and allows for a simpler linear analysis. Similarly, this model does not account for any rotor translation along or rotation about the axis of the flywheel, except that the gyroscopic stiffness increases

with increasing rotor speed. The bearings in this model are assumed to be linear springs, as opposed to the controllable magnetic bearings of an actual IPACS.

Even the best control model will be unable to completely filter out all disturbances such as rotor imbalance due to limitations such as signal bandwidth and control saturation. This model assumes a small residual amount of rotor imbalance that cannot be filtered out and examines the interactions between multiple residual imbalances. Therefore, the input and output forces are small.

The scope of this analysis is also limited to rigid flywheel rotors. There are higher bending modes associated with flexible rotors, but the first four vibration modes discussed in Section 2.3.5 are dominant—bending modes are typically above a frequency of 1 kHz (15:35).

III. Methodology

3.1 Overview

This thesis will use an analytical model to study the vibration interaction of multiple gyroscopes. Vibrations can come from several sources, but this thesis will examine only those caused by unbalanced flywheels. The model will be numerically integrated using the `ode45` command in MATLAB®.

3.2 Model Description

3.2.1 Model Construction. The model used in this thesis is a system of two flywheels and a support structure as shown in Figure 10. The flywheels are axially aligned, with opposite spin directions. The flywheels are arranged such that the system COM and the support COM are co-located.

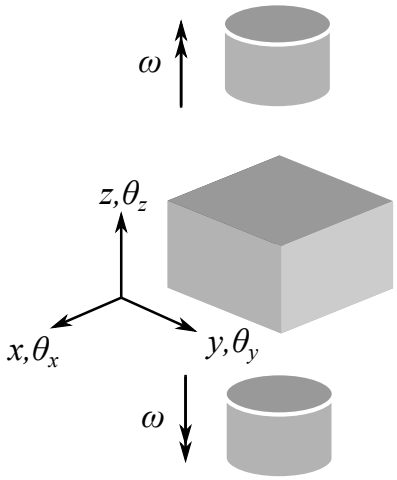

Figure 10: Basic configuration of the model used in this thesis

The flywheels are each connected to the support structure with two magnetic bearings, as shown in Figure 11. Flywheels of length l and radius r are located at distance d from the support COM and supported at each end by a magnetic bearing. The magnetic bearings have only translational stiffness, but having one of them at

each end of the rotor will create an effective rotational stiffness. The stiffnesses in the transverse (x and y) and axial (z) directions are separate and not necessarily related. In this thesis, however, axial displacements are ignored, so the axial stiffness is unimportant. When damping is accounted for in this thesis, all springs shown represent bearings with both stiffness and damping.

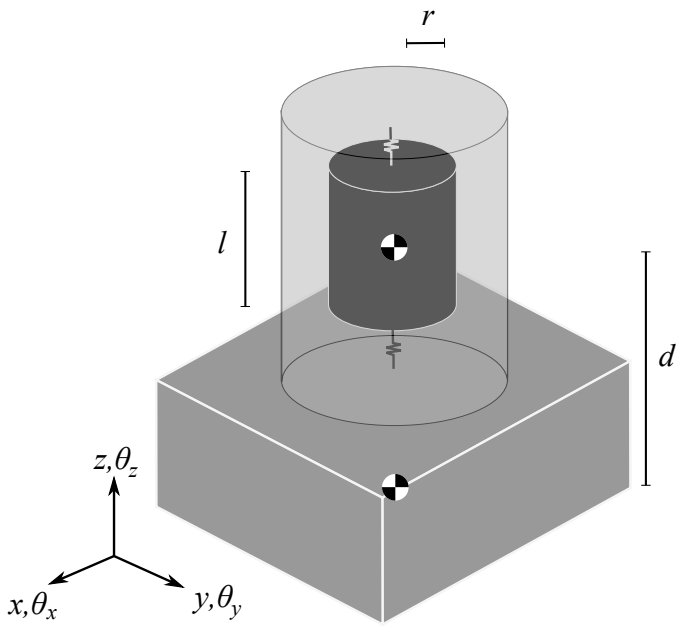

Figure 11: Flywheel in housing connected to IPACS support structure

The model is simplified by replacing each body with a point mass as shown in Figure 12. There is one 4 degree of freedom (DOF) spring (and damper) located at the flywheel's COM, which is attached to the support structure with a rigid link. The spring shown has transverse translational (x and y) and rotational (θ_x and θ_y) stiffness.

For a flywheel of length l with individual magnetic bearing stiffness k_{mag}, the model will have linear stiffness $k_{model} = 2k_{mag}$ and transverse rotational stiffness $\kappa_{T,model} = \frac{1}{2}k_{mag}l^2$ (22:125). Damping is similar: $c_{model} = 2c_{mag}$ and $C_{T,model} = \frac{1}{2}c_{mag}l^2$.

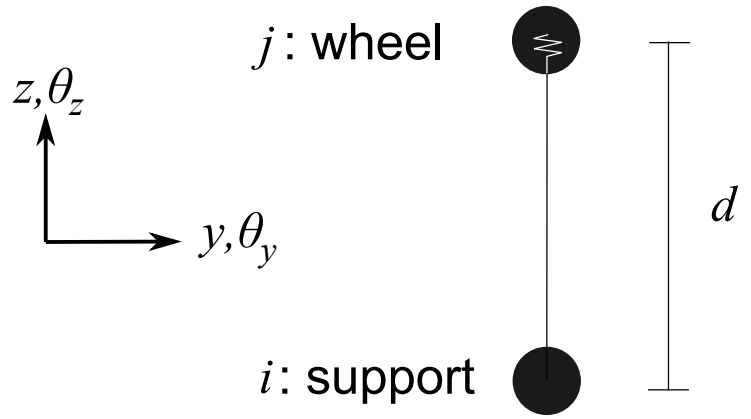

Figure 12: Model of support/flywheel connection. Bodies are point masses separated by distance d

The two flywheels are attached to the support structure as discussed previously and illustrated again in Figure 13. Also shown is a connection to the satellite, which represents a soft mount between the support structure and the rest of the satellite. Since all forces studied are periodic or symmetric about the system and support structure COM, the support will primarily experience rotations rather than translations. For this reason, the satellite/support spring is modeled as a 3 DOF spring with only rotational stiffness. The satellite in this model is assumed to be heavy enough that it can be considered fixed. For most validation runs, the satellite/support spring was turned off to allow free rotation of the satellite.

Finally, an appendage can be added to the model. The appendage represents a flexible spacecraft structure such as a solar array or antenna, and it is used to study low frequency excitation. The appendage is shown in Figure 14. The appendage and support structure COMs are co-located, and they are connected by a 2 DOF spring with only transverse (θ_x and θ_y) rotational stiffness.

3.2.2 Model Inputs. The sources of vibration in this model will be rotor imbalances. Real rotors can have very small imbalances if they are manufactured

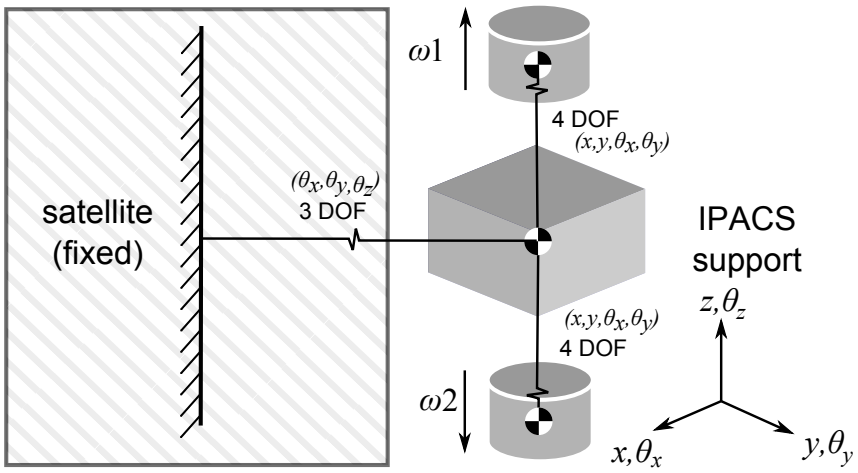

Figure 13: System model with satellite included. The satellite/support spring can be turned off if needed

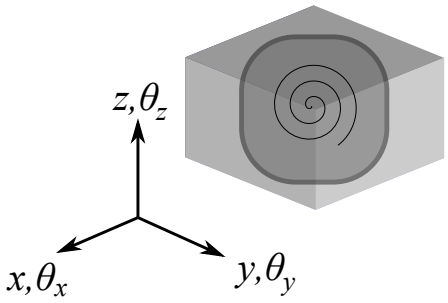

Figure 14: Model of appendage, which is connected to the support structure with only a rotational spring

with tight tolerances, but imbalances will always be present after manufacturing. The rotors in this model will be assumed to be imbalanced in such a way that they cause a purely two-dimensional vibration: linear (in x, y) or rotational (in θ_x, θ_y). These imbalances are shown conceptually in Figure 15. The axially symmetric imbalances in a real rigid rotor can be described as a combination of these two imbalances, but they will be examined individually in this model.

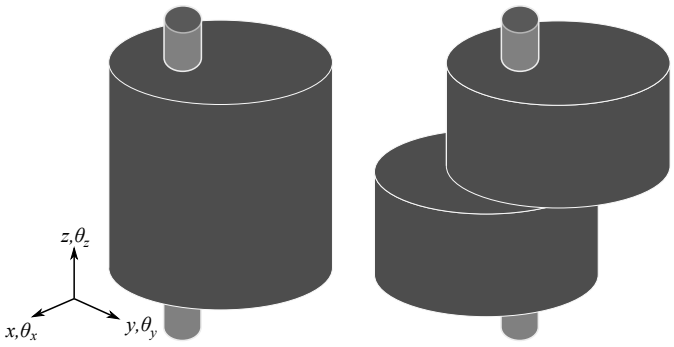

(a) Linear (b) Rotational

Figure 15: Two sources of axially-symmetric imbalance-induced vibration

The rotating imbalance creates a centripetal force as discussed in Section 2.3.4. For this model the rotor eccentricities are replaced with an ideal rotor plus periodic input forces synchronized with wheel position and proportional to eccentricity and the square of the wheel speed.

3.2.3 Model Parameters. The flywheel for this model is a theoretical flywheel only, but it is intended to be realistically sized. Flywheel parameters are given in Table 1.

Magnetic bearing stiffness and damping are similar to those used in some NASA studies (4). The nominal mass properties are described in Hibbeler's text (8). They are defined here in such a way that they describe a short rotor $\left(P = \frac{I_T}{I_P} > 1\right)$ to study super-synchronous whirl. When necessary, I_T is changed to adjust the rotor parameter

Table 1: Flywheel model parameters

mag bearing stiffness	k_{mag}	1756	kN/m
mag bearing damping	c_{mag}	3.512	kN/m/s
rotor mass	m	10	kg
rotor length	l	20	cm
support/rotor distance	d	15	cm
rotor radius	r	15	cm
rotor shaft/COM distance	ρ	0.01	nm
model translational stiffness	k_{model}	3512	kN/m
model rotational stiffness	κ_{model}	35.12	kN-m/rad
model translational damping	c_{model}	7.024	kN/m/s
model rotational damping	C_{model}	70.24	N-m/rad/s
transverse MOI	I_T	0.0896	kg-m^2
polar MOI	I_P	0.1125	kg-m^2
rotor MOI ratio	P	1.2558	-

P. This adjustment is made to study longer rotors when looking for sub-synchronous whirl. The COM–shaft offset distance, ρ was chosen to give similar disturbance inputs to the residual disturbances found by Park (15:87). The mass properties of the support structure are shown in Table 2.

Table 2: Support structure parameters

mass	m	10	kg
MOI	$I_{x,y,z}$	10	kg-m^2

3.3 System Equation of Motion

3.3.1 System Equation of Motion Components. When a system of independent, unconnected, gyroscopic rigid bodies is described in state-space as shown in Equation 2, it takes the form of the block diagonal matrix shown in Equation 17. The stiffness and damping terms here represent each body being connected to a fixed body.

$$\dot{\boldsymbol{q}} = \begin{bmatrix} \mathbf{A}_1 & \dots & \mathbf{0} \\ \vdots & \ddots & \vdots \\ \mathbf{0} & \dots & \mathbf{A}_n \end{bmatrix} \boldsymbol{q} + \begin{bmatrix} \mathbf{B}_1 \\ \vdots \\ \mathbf{B}_n \end{bmatrix} \boldsymbol{u} \tag{17}$$

where the state vector $\boldsymbol{q} = \begin{bmatrix} \boldsymbol{q_1}^{\mathrm{T}} & \dots & \boldsymbol{q_n}^{\mathrm{T}} \end{bmatrix}^{\mathrm{T}}$, $\boldsymbol{q_i} = \begin{bmatrix} \boldsymbol{r_i}^{\mathrm{T}} & \boldsymbol{\theta_i}^{\mathrm{T}} & \boldsymbol{v_i}^{\mathrm{T}} & \boldsymbol{\omega_i}^{\mathrm{T}} \end{bmatrix}^{\mathrm{T}}$, and $\mathbf{A}_i$ and $\mathbf{B}_i$ are defined according to Equations 18 and 19, similar to Equation 4. $\boldsymbol{r_i}$ and $\boldsymbol{\theta_i}$ are the position (x, y, z) and rotation $(\theta_x, \theta_y, \theta_z)$ vectors of the bodies, respectively, and $\boldsymbol{v_i}$ and $\boldsymbol{\omega_i}$ are the corresponding translational and rotational velocities.

$$\mathbf{A}_i = \begin{bmatrix} \mathbf{R}_i \end{bmatrix} \begin{bmatrix} \mathbf{0} & \mathbf{I} \\ \mathbf{M}_i^{-1}\mathbf{K}_i & \mathbf{M}_i^{-1}(\mathbf{C}_i + \mathbf{G}_i) \end{bmatrix} \begin{bmatrix} \mathbf{R}_i^{\mathrm{T}} \end{bmatrix} \tag{18}$$

$$\mathbf{B}_i = \begin{bmatrix} \mathbf{R}_i \end{bmatrix} \begin{bmatrix} \mathbf{0} \\ \mathbf{M}_i^{-1}\mathbf{B}_i \end{bmatrix} \begin{bmatrix} \mathbf{R}_i^{\mathrm{T}} \end{bmatrix} \tag{19}$$

A system of connected rigid bodies is described by the same equation of motion given in Equation 17 plus the addition of non-block diagonal stiffness terms in the $\mathbf{A}$ matrix. In the case of this model, the stiffness between each flywheel and the support structure is identical in the local axially aligned frame. This common stiffness matrix can be derived using the spring equation with the help of a diagram of system displacements. With the support and the wheel modeled as point masses, a simple diagram of displacements in x is shown in Figure 16, which is a simplification of the housing support structure. Small angles are assumed.

Figure 16 is used to determine the inter-body spring forces caused by system displacements according to $F = -kx$. The bodies are modeled as point masses. Angles

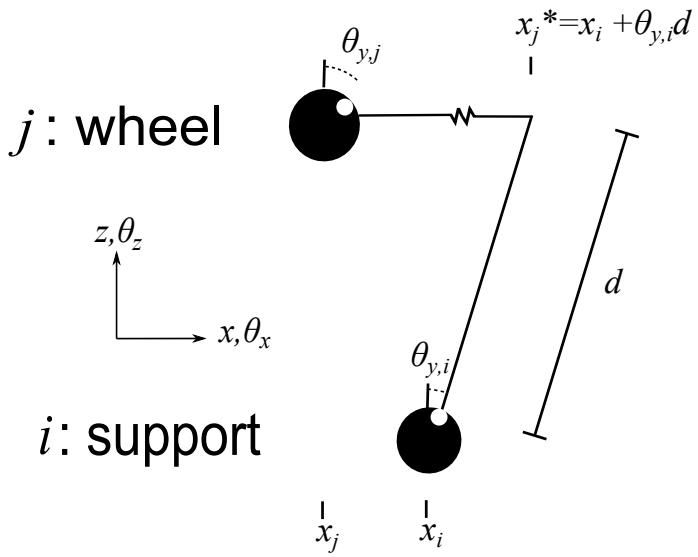

Figure 16: System displacements in x. Bodies i and j are point masses. This diagram is used to determine spring forces between bodies i and j in the x direction. The flywheel (j) is attached to the end of a rigid link length d extending from the support structure (i)

are assumed to be small, so $\sin\theta \approx \theta$ and $\cos\theta \approx 1$. x_j^* describes the displacement of the rotor support structure in the x direction. The rotor's position in x is defined as x_j. The x direction resultant spring force on mass i due to the displacements shown in Figure 16 is given below in Equation 20.

$$\Sigma F_x = -k_x(x_i + \theta_{y,i}d - x_j) \tag{20}$$

Simlarly, the resultant torques on mass i about the y axis are described below in Equation 21.

$$\Sigma T_y = -\kappa_y(\theta_{y,i} - \theta_{y,j}) - kd(\theta_{y,i}d + x_i - x_j) \tag{21}$$

The remaining resultant forces and torques on mass i can be determined by analogy or by the construction of a similar diagram. The forces and torques on mass i in y and θ_x are shown below in Equation 22. Since this model ignores rotor motion in z and θ_z, those equations are not listed.

$$\begin{aligned} \Sigma F_y &= -k_y(y_i - \theta_{x,i}d - y_j) \\ \Sigma T_x &= -\kappa_x(\theta_{x,i} - \theta_{x,j}) - kd(\theta_{x,i}d - y_i + y_j) \end{aligned} \tag{22}$$

Likewise, the forces acting on mass j (the flywheel) are shown below in Equation 23.

$$\begin{aligned} \Sigma F_x &= -k_x(x_j - x_i - \theta_{y,i}d) \\ \Sigma F_y &= -k_y(y_j - y_i + \theta_{x,i}d) \\ \Sigma T_x &= -\kappa_x(\theta_{x,j} - \theta_{x,i}) \\ \Sigma T_y &= -\kappa_y(\theta_{y,j} - \theta_{y,i}) \end{aligned} \tag{23}$$

Equations 20–23 can be represented in matrix form as shown in Equation 24 where i, j are the bodies being connected. They describe the forces applied to the bodies by various system displacements.

$$\begin{bmatrix} \boldsymbol{f}_i \\ \boldsymbol{f}_j \end{bmatrix} = \left[\begin{array}{c|c} \mathbf{K}_{i,i} & \mathbf{K}_{i,j} \\ \hline \mathbf{K}_{j,i} & \mathbf{K}_{j,j} \end{array}\right] \begin{bmatrix} \boldsymbol{q}_i \\ \boldsymbol{q}_j \end{bmatrix} \tag{24}$$

$$\mathbf{K}_{i,i} = \begin{bmatrix} -k_T & 0 & 0 & 0 & -k_T d & 0 \\ 0 & -k_T & 0 & k_T d & 0 & 0 \\ 0 & 0 & 0 & 0 & 0 & 0 \\ 0 & k_T d & 0 & -k_T d^2 - \kappa_T & 0 & 0 \\ -k_T d & 0 & 0 & 0 & -k_T d^2 - \kappa_T & 0 \\ 0 & 0 & 0 & 0 & 0 & 0 \end{bmatrix}$$

$$\mathbf{K}_{i,j} = \begin{bmatrix} k_T & 0 & 0 & 0 & 0 & 0 \\ 0 & k_T & 0 & 0 & 0 & 0 \\ 0 & 0 & 0 & 0 & 0 & 0 \\ 0 & -k_T d & 0 & \kappa_T & 0 & 0 \\ k_T d & 0 & 0 & 0 & \kappa_T & 0 \\ 0 & 0 & 0 & 0 & 0 & 0 \end{bmatrix}$$

$$\mathbf{K}_{j,i} = \mathbf{K}_{m,n}^{\mathrm{T}}$$

$$\mathbf{K}_{j,j} = \begin{bmatrix} -k_T & 0 & 0 & 0 & 0 & 0 \\ 0 & -k_T & 0 & 0 & 0 & 0 \\ 0 & 0 & 0 & 0 & 0 & 0 \\ 0 & 0 & 0 & -\kappa_T & 0 & 0 \\ 0 & 0 & 0 & 0 & -\kappa_T & 0 \\ 0 & 0 & 0 & 0 & 0 & 0 \end{bmatrix}$$

For this model, mass i is always the support structure, so $i \equiv 1$. This 12 x 12 stiffness matrix is separated into four parts which are placed into the global system **A** matrix in the appropriate locations.

The damping matrix, $\mathbf{C}$, is treated the same way. This model uses damping proportional to stiffness to represent the losses in the system. This is represented by $\mathbf{C} = \xi\mathbf{K}$, where $\xi = 0.002$, which is reflected by the values in Table 1.

3.3.2 System Equation of Motion Assembly. Recalling Equations 2 and 17, a state-space system EOM is written as

$$\dot{\boldsymbol{q}} = \mathbf{A}\boldsymbol{q} + \mathbf{B}\boldsymbol{u}$$

Both $\mathbf{A}$ and $\mathbf{B}$ are assembled from their component parts, which are described in Section 3.3.1. This can also be represented as shown in Equations 25 and 26.

$$\mathbf{A} = \mathbf{M}_{\mathbf{system}}^{-\mathbf{1}} \left(\mathbf{A}_{\mathbf{G}} + \mathbf{A}_{\mathbf{K}} + \mathbf{A}_{\mathbf{C}}\right) \tag{25}$$

$$\mathbf{B} = \mathbf{M}_{\mathbf{system}}^{-\mathbf{1}} \mathbf{B}_{\mathbf{system}} \tag{26}$$

where

$$\mathbf{M}_{\mathbf{system}}^{-\mathbf{1}} = \begin{bmatrix} \mathbf{I} & \mathbf{0} & & & \\ \mathbf{0} & \mathbf{M}_1^{-1} & & & \\ & & \ddots & & \\ & & & \mathbf{I} & \mathbf{0} \\ & & & \mathbf{0} & \mathbf{M}_n^{-1} \end{bmatrix}$$

$$\mathbf{A_G} = \begin{bmatrix} \mathbf{0} & \mathbf{I} & & & \\ \mathbf{0} & \mathbf{G}_1 & & & \\ & & \ddots & & \\ & & & \mathbf{0} & \mathbf{I} \\ & & & \mathbf{0} & \mathbf{G}_n \end{bmatrix}$$

$$\mathbf{A_K} = \begin{bmatrix} \mathbf{0} & \mathbf{0} & \mathbf{0} & \mathbf{0} & & \mathbf{0} & \mathbf{0} \\ \Sigma\mathbf{K}_{1,1} & \mathbf{0} & \mathbf{K}_{1,2} & \mathbf{0} & & \mathbf{K}_{1,n} & \mathbf{0} \\ \mathbf{0} & \mathbf{0} & \mathbf{0} & \mathbf{0} & & \mathbf{0} & \mathbf{0} \\ \mathbf{K}_{2,1} & \mathbf{0} & \Sigma\mathbf{K}_{2,2} & \mathbf{0} & & \mathbf{K}_{2,n} & \mathbf{0} \\ & & & & \ddots & & \\ \mathbf{0} & \mathbf{0} & \mathbf{0} & \mathbf{0} & & \mathbf{0} & \mathbf{0} \\ \mathbf{K}_{n,1} & \mathbf{0} & \mathbf{K}_{n,2} & \mathbf{0} & & \Sigma\mathbf{K}_{n,n} & \mathbf{0} \end{bmatrix}$$

$$\mathbf{A_C} = \begin{bmatrix} \mathbf{0} & \mathbf{0} & \mathbf{0} & \mathbf{0} & & \mathbf{0} & \mathbf{0} \\ \mathbf{0} & \Sigma\mathbf{C}_{1,1} & \mathbf{0} & \mathbf{C}_{1,2} & & \mathbf{0} & \mathbf{C}_{1,n} \\ \mathbf{0} & \mathbf{0} & \mathbf{0} & \mathbf{0} & & \mathbf{0} & \mathbf{0} \\ \mathbf{0} & \mathbf{C}_{2,1} & \mathbf{0} & \Sigma\mathbf{C}_{2,2} & & \mathbf{0} & \mathbf{C}_{2,n} \\ & & & & \ddots & & \\ \mathbf{0} & \mathbf{0} & \mathbf{0} & \mathbf{0} & & \mathbf{0} & \mathbf{0} \\ \mathbf{0} & \mathbf{C}_{n,1} & \mathbf{0} & \mathbf{C}_{n,2} & & \mathbf{0} & \Sigma\mathbf{C}_{n,n} \end{bmatrix}$$

Subscripts on stiffness and damping terms are the i, j subscripts found in Equation 24. Placement of each term is determined from Equation 18. $\mathbf{A_K}$ and $\mathbf{A_C}$ of Equation 25 are more general than the model requires. Since the only connections in the model are between body 1 (the support structure) and other bodies, many of the terms shown in these general equations are unnecessary, leading to the simplification of $\mathbf{A_K}$ as $\mathbf{A_K}^*$ as shown below, where all of the off-diagonal terms not along the first row or column are zero. $\mathbf{A_C}^*$ is similar. The stiffness term for the support structure, $\Sigma\mathbf{K}_{1,1}$, also contains the stiffness between the fixed satellite bus and the support structure.

$$\mathbf{A_K}^* = \begin{bmatrix} \mathbf{0} & \mathbf{0} & \mathbf{0} & \mathbf{0} & & \mathbf{0} & \mathbf{0} \\ \Sigma\mathbf{K}_{1,1} & \mathbf{0} & \mathbf{K}_{1,2} & \mathbf{0} & & \mathbf{K}_{1,n} & \mathbf{0} \\ \mathbf{0} & \mathbf{0} & \mathbf{0} & \mathbf{0} & & \mathbf{0} & \mathbf{0} \\ \mathbf{K}_{2,1} & \mathbf{0} & \mathbf{K}_{2,2} & \mathbf{0} & & \mathbf{0} & \mathbf{0} \\ & & & & \ddots & & \\ \mathbf{0} & \mathbf{0} & \mathbf{0} & \mathbf{0} & & \mathbf{0} & \mathbf{0} \\ \mathbf{K}_{n,1} & \mathbf{0} & \mathbf{0} & \mathbf{0} & & \mathbf{K}_{n,n} & \mathbf{0} \end{bmatrix}$$

The input matrix $\mathbf{B}$ is simpler. It links each of the states with an input u_n. The column and row of a $\mathbf{B}$ term determine which input force is applied to which state, respectively. Because the EOM is represented in the second half of each body's state vector, that is where the inputs are applied.

$$\mathbf{B_{system}} = \begin{bmatrix} \mathbf{0} \\ \mathbf{B}_1 \\ \vdots \\ \mathbf{0} \\ \mathbf{B}_n \end{bmatrix} \tag{27}$$

This model incorporates rotating centripetal force inputs synchronized to the rotation of each flywheel. The input vector describing each of these terms is shown in Equation 28.

$$\boldsymbol{u} = \begin{bmatrix} e_1\omega_1^2 \sin\theta_1 t & e_1\omega_1^2 \cos\theta_1 t & \dots & e_n\omega_n^2 \sin\theta_n t & e_n\omega_n^2 \cos\theta_n t & 1 \end{bmatrix}^{\mathrm{T}} \tag{28}$$

As Equation 28 shows, the input vector has two centripetal force terms for each wheel, and they are 90° out of phase from each other. The magnitude of the force is $e_i\omega_i^2$, and the force acts in the direction of the current wheel rotation, θ_i. In the model this is divided into x and y (or θ_x and θ_y) inputs, which vary periodically with $\sin\theta_i$ and $\cos\theta_i$. The last term, 1, is used to allow for a constant force input for validation purposes. This vector is used for all model input. Different system input cases are created by applying forces (imbalances or a constant force) to various states with changes in the input matrix $\mathbf{B}$.

3.4 Integration

The model created in MATLAB® is integrated numerically using `ode45`. The differential equation created by the state-space model is kept as small as possible because it must be integrated over many iterations. Some components of the system

EOM, however, are functions of time. Both the gyroscopic matrix $\mathbf{G}$ and the force vector $\boldsymbol{u}$ are time dependent and they must be recomputed for each iteration of the integration.

In addition, careful attention must be paid to the application of rotating input forces. A periodic rotating input force is represented in two linear dimensions as a sine wave in one dimension and a cosine wave in the other dimension. If these forces are directly applied to an unconstrained mass initially at rest, they can cause a secular drift in one direction. This phenomenon occurs in the model used for this thesis (but not the actual system). One solution to minimize the effect of the secular drift is described in Appendix A.

3.5 Additional Components

3.5.1 Appendage. The addition of a flexible appendage is accommodated by adding another body to the model. An appendage is used to study the beat phenomenon as it applies to this model. Since the studied effects of this appendage are limited to θ_x and θ_y, the appendage is only connected to the model with torsional springs. Also, the only relevant mass properties are I_x and I_y. These properties, which were chosen to give the appendage a natural frequency of 5 Hz, are shown in Table 3.

Table 3: Appendage mass properties

mass	$I_{x,y}$	10	kg-m^2
transverse MOI	κ_T	9869	N-m/rad

In the model, the appendage is added as a new body with mass $\mathbf{M_{app}} = \text{diag}\left(\begin{bmatrix}1 & 1 & 1 & 10 & 10 & 1\end{bmatrix}\right)$ and stiffness $\mathbf{K_{app}}$ defined according to Equation 24, with all terms except κ_T

3.5.2 Satellite/support spring. When required, a spring is connected between a firm fixed satellite and the support structure. Since input forces are cyclical and cause primarily rotations in the support structure, it is the rotational DOFs that become problematic and require constraints. This additional spring is attached to $\mathbf{K_{1,1}}$, as discussed in Section 3.3.2, and takes the form $\mathbf{K_{support}} = -1\times10^{6}\text{diag}\left(\begin{bmatrix}0 & 0 & 0 & 1 & 1 & 0\end{bmatrix}\right)$.

3.6 Validation

3.6.1 Validation Inputs. A simple IPACS model was created for validation purposes. The flywheel properties for this model are shown in Table 4. This model has a long rotor, so it will have a critical coning speed.

Table 4: Validation model flywheel properties

rotor mass	m	10	kg
rotor length	l	0.5	m
rotor radius	r	0.12	m
support/rotor distance	d	1	m
mag bearing stiffness	k_{mag}	2500	N/m
polar MOI	I_P	0.0781	kg-m^2
transverse MOI	I_T	0.2474	kg-m^2
rotor MOI ratio	P	0.3158	

For validation, several test inputs were given to the model and the responses were verified. First, a few constant-direction forces were applied to ensure that signs were correct and that the model components were assembled correctly. Exponential rotational growth due to a constant applied torque is shown in Figure 17. Figure 17 and all similar figures show a time history of each system displacement for each wheel. All responses are shown in global coordinates.

The next set of tests were performed to ensure the model's consistency in accounting for wheel spin direction. One wheel at a time was given an imbalance input

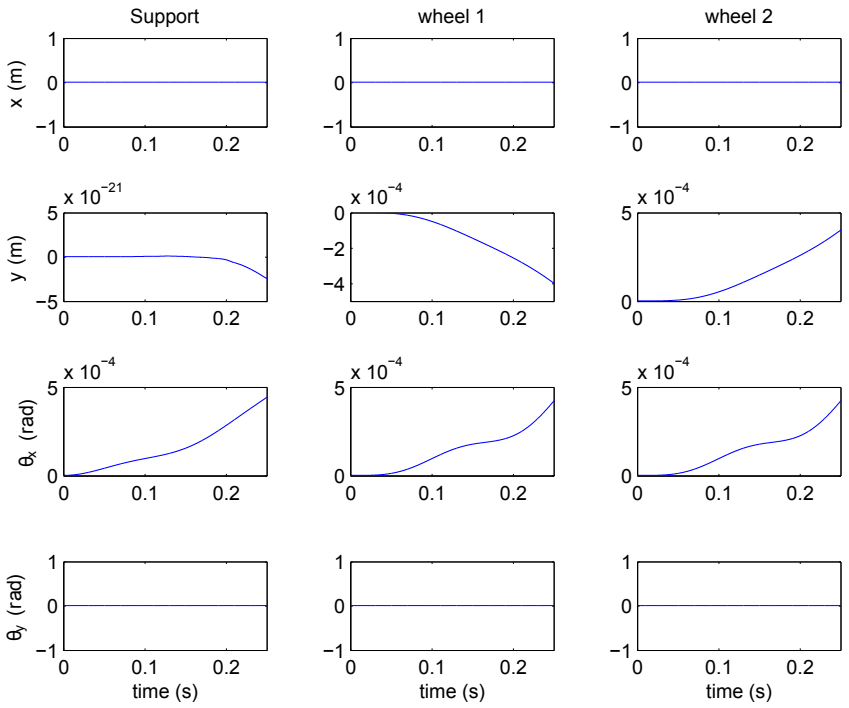

(a) Wheel speed: 0

(b) Input force: as shown

Figure 17: System demonstrating exponential displacement growth due to a constant torque input applied to θ_x

to test the response of that wheel and the system. These tests are shown in Figures 18 and 19. In both figures, the whole system is rotating together slowly as a result of the rotating imbalance, as expected.

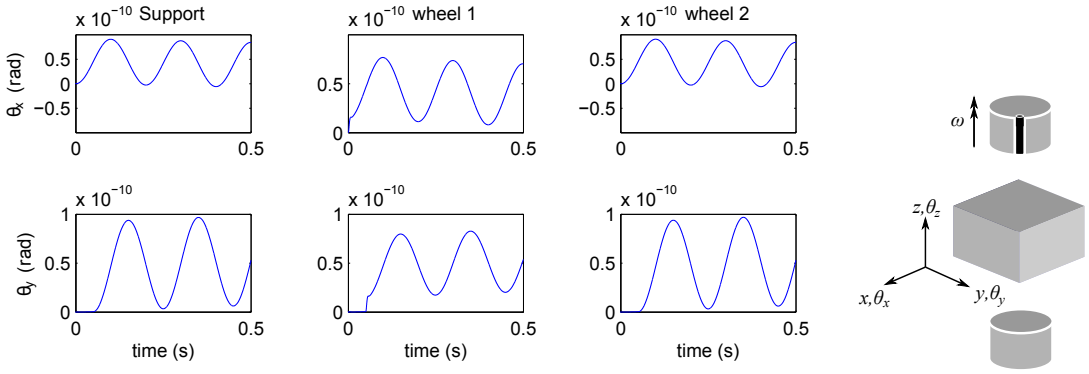

(a) Wheel speed: 0/5 RPS as shown

(b) Input force: as shown

Figure 18: System demonstrating forward whirl

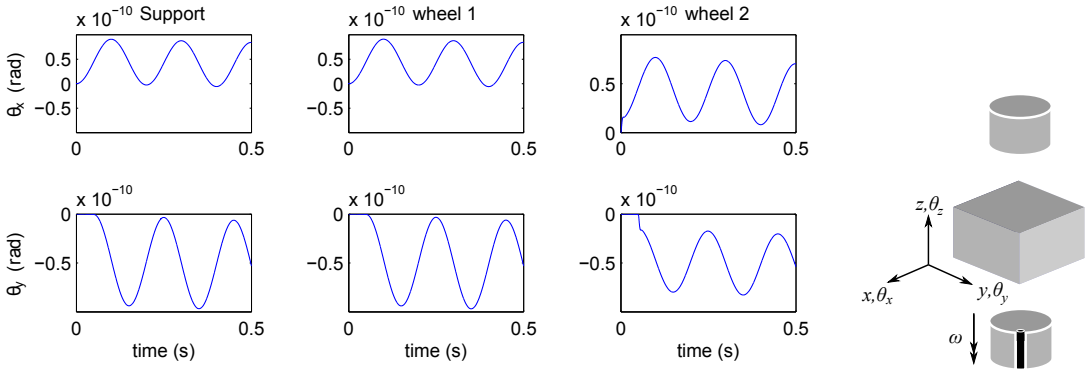

(a) Wheel speed: 5/0 RPS as shown

(b) Input force: as shown

Figure 19: System demonstrating backward whirl

The 90° phase shift between the θ_x and θ_y rotations reveals that this vibration is a coning motion. When θ_x leads θ_y, as seen in Figure 18, the system is whirling counter-clockwise as viewed from "above" (looking from the positive z direction towards the origin). This motion is a forward whirl for wheel 1, since that rotor is spinning in this direction. It is a backward whirl for wheel 2, since the nominal spin direction of

rotor 2 is opposite that of wheel 1. When θ_y leads θ_x, the system is rotating in the opposite direction and the whirl orientations are reversed. This response was studied with the normal system model, not the validation model.

Next the system's natural frequencies were examined. The first three natural frequencies of a rotor-bearing system are given in Equations 11–13 and 15. Recall that $f_1 = f_2$ are bouncing modes, and f_3 and f_4 are forward and backward whirling modes. The system responses demonstrating f_1–f_4 are shown in Figures 20–24. Figure 20 demonstrates the bouncing mode $f_1 = f_2$.

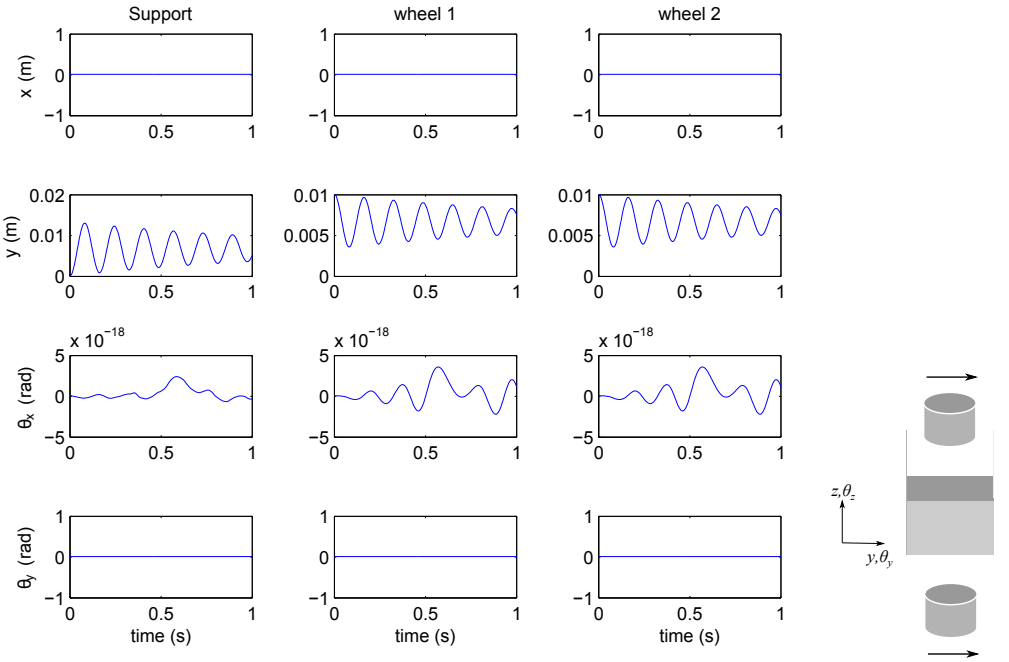

(a) Wheel speed: zero

(b) Initial state: as shown

Figure 20: System demonstrating bouncing vibration at $f_1 \approx 6.16$ Hz

Equation 11 gives the natural frequency of a spring-mass system as $f_1 = \sqrt{k/m}/2\pi$. The model's two flywheels were displaced symmetrically to make the system equivalent to a free two-body system. The equivalent mass of a freely vibrating two-body system can be found by $m_{eq} = \left(\sum_{i=1}^{n} m_i^{-1}\right)^{-1}$. With a 10 kg support structure and two 10 kg flywheels, the system equivalent mass is 6.66 kg and $f_1 = f_2 \approx 6.16$ Hz.

Figure 21 shows the expected forward and backward whirl speeds of the validation model. By inspection, when wheel speed is zero, $f_3 = f_4 \approx 5.66$ Hz, which agrees with Equation 12. At a wheel speed of 10 RPS, $f_3 \approx 7.36$ Hz and $f_4 \approx 4.40$ Hz.

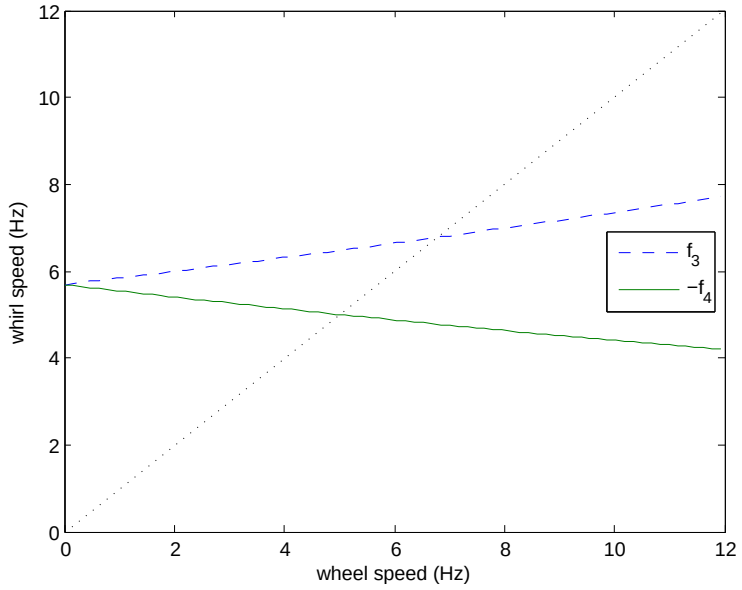

Figure 21: Whirl modes of the validation system. Dotted line is synchronous with wheel speed

Figure 22 shows that the forward whirl mode behaves as expected with flywheel speed $\omega = 0$. Backward whirl at this speed is identical except for direction, which appears as an opposite phase difference in θ_x and θ_y.

The whirl modes are dependent on wheel speed and they diverge with increasing wheel speed. Figures 23 and 24 show the whirl modes when wheel speed is 10 RPS. $f_3(10 \text{ Hz}) \approx 7.36$ Hz and $f_4(10 \text{ Hz}) \approx 4.40$ Hz. In both cases the system whirl is in the same direction (counter-clockwise as viewed from "above"), but the wheel speed directions were changed as necessary to make these forward or backward whirling motions.

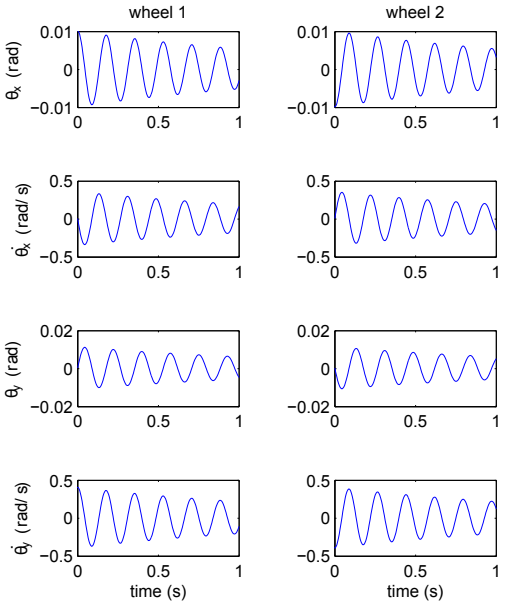

(a) Wheel speed: 0

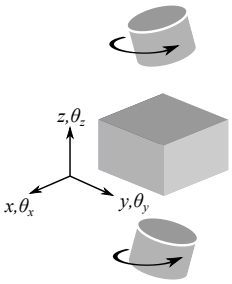

(b) Initial state: as shown

Figure 22: Forward whirl with zero wheel speed: $f_3 = f_4 \approx 5.66$ Hz. Backward whirl is identical except for direction

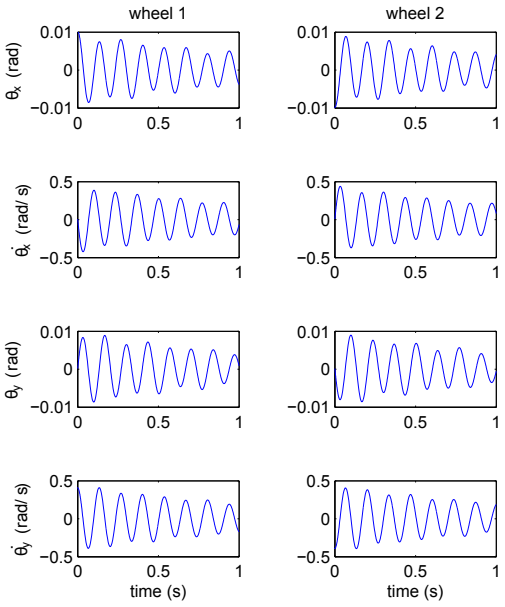

(a) Wheel speed: 10 RPS as shown

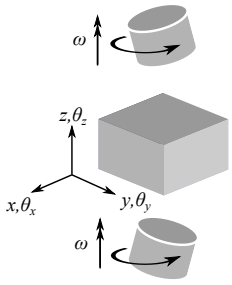

(b) Initial state: as shown

Figure 23: Forward whirl mode at $f_3 \approx 7.36$ Hz when wheel speed is 10 RPS

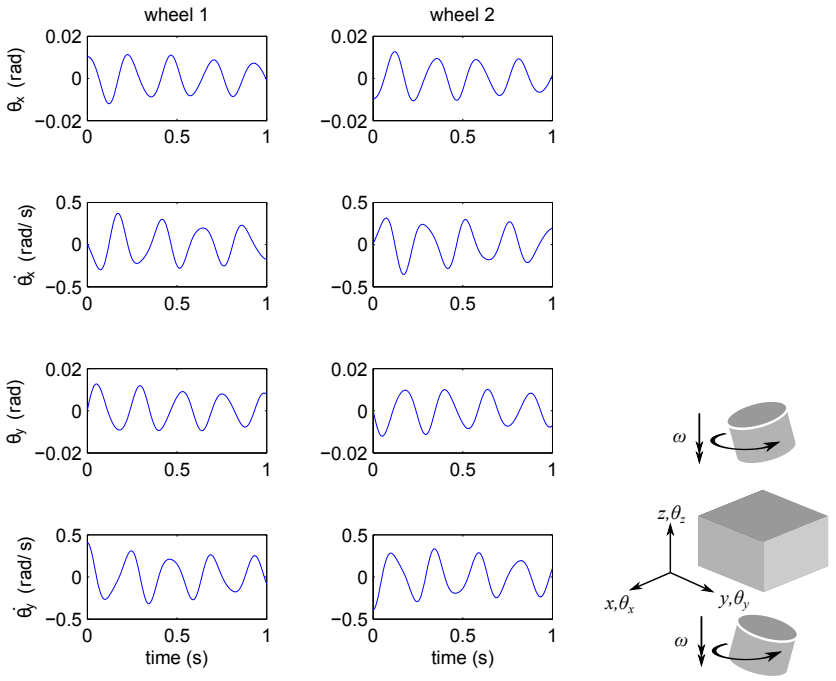

(a) Wheel speed: 10 RPS as shown

(b) Initial state: as shown

Figure 24: Backward whirl mode at $f_4 \approx 4.40$ Hz when wheel speed is 10 RPS

Forward whirl f_3 is speed dependent and, for a long rotor, there is a critical coning speed where the whirling frequency is the same as the wheel frequency. Figure 25 demonstrates this phenomenon. Wheel speed is varied from 4–12 RPS, and vibration is much worse at the critical coning frequency $f_{con} \approx 6.8$ Hz. The difference between the support structure's vibration in θ_x and θ_y is a modeling artifact.

3.7 Summary

The model developed for this thesis was tested and performed correctly given a variety of input scenarios, including initial conditions, constant forces, and periodic forces. Critical coning frequency was demonstrated successfully, as well as forward and backward whirls.

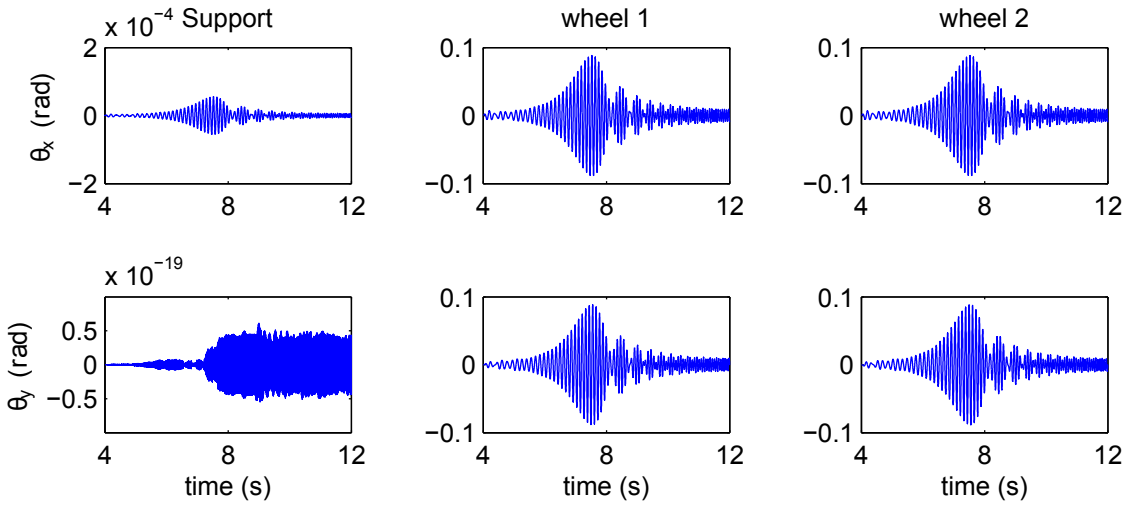

Figure 25: Model demonstrating the critical coning frequency. As the wheel speed passes through $f_{con} \approx 6.8$ Hz, the vibration amplitude gets much larger. Wheel speed varies linearly from 4 RPS at t=4 to 12 RPS at t=12

IV. Results and Analysis

Several tests were conducted using the model described in this thesis, and the results are presented here. First, a full frequency sweep was performed to see if any immediate problems arose. Other tests examined the existence of beat phenomenon and extra-synchronous whirl excitation. For this section, flywheel-specific rotation speed is represented as ω_n.

4.1 Full Envelope Sweep

First a variety of full envelope frequency sweep tests were carried out. For these tests, wheel speed of one or both rotors varied from 333–1000 RPS. A moment-inducing imbalance in each rotor caused a vibration input synchronized with each wheel speed.

These tests revealed nothing of interest except that the system's gyroscopic stiffness diminishes as the wheel speeds approach equality in opposite directions. This reduction in gyroscopic stiffness is illustrated nicely in Figures 26–28.

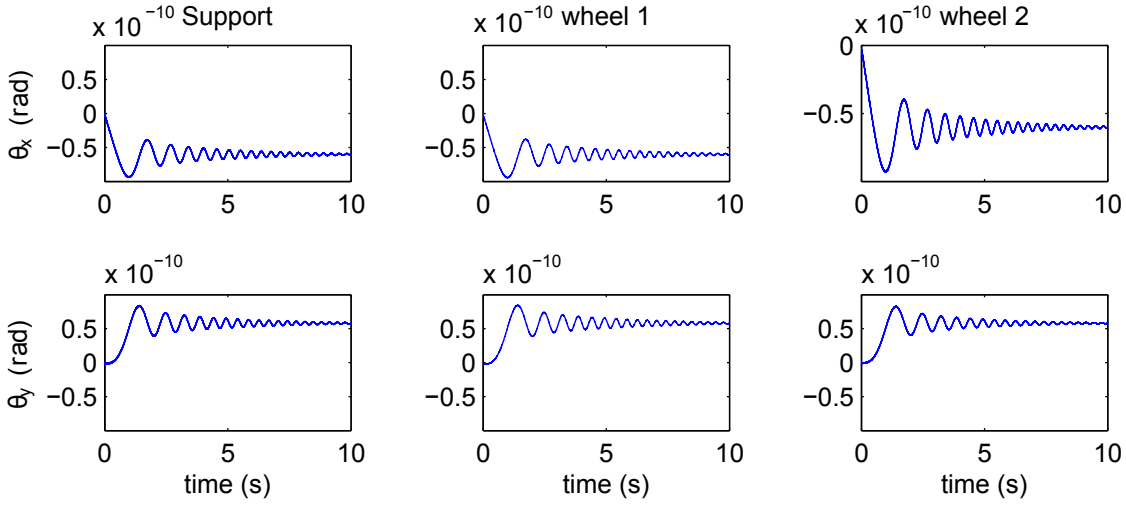

Figure 26: System rotations as a result of moment-inducing imbalance vibrations. Wheel speeds: $\omega_1 = 333$, $\omega_2 = 333$–1000 RPS

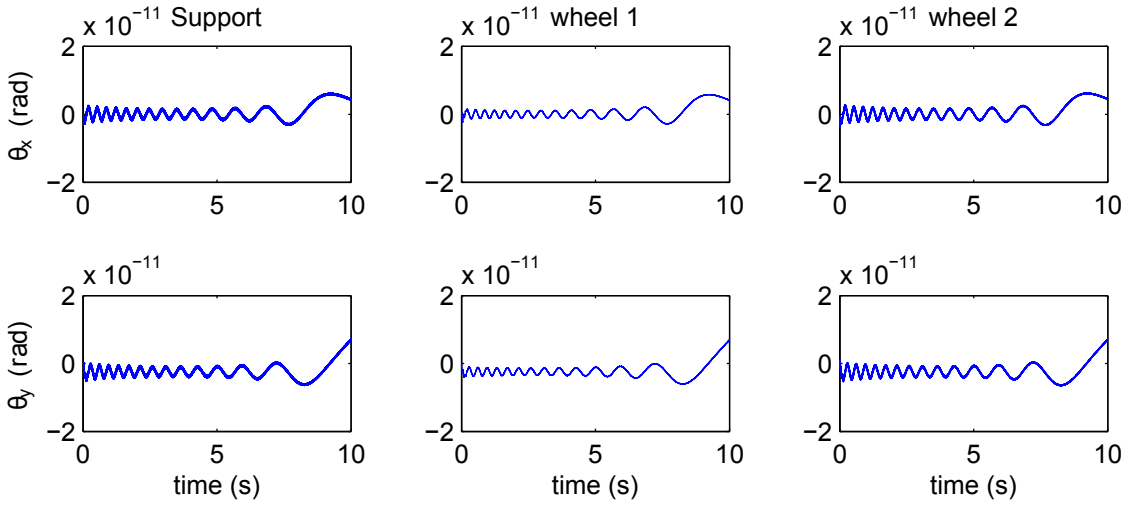

Figure 27: System rotations as a result of moment-inducing imbalance vibrations. Wheel speeds: Wheel speeds: $\omega_1 = 1000$, $\omega_2 = 333$–1000 RPS

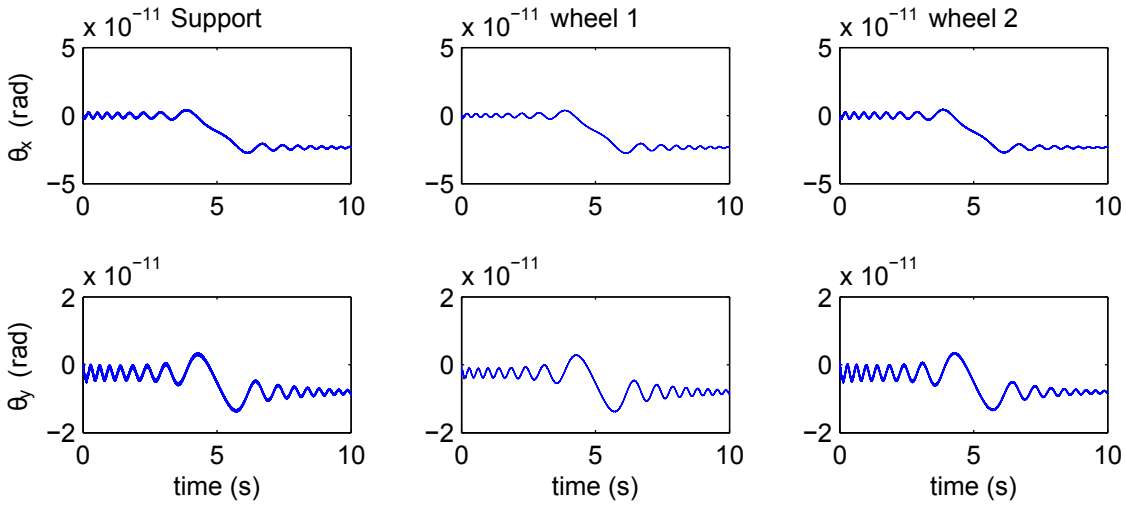

Figure 28: System rotations as a result of moment-inducing imbalance vibrations. Wheel speeds: $\omega_1 = 1000$–333, $\omega_2 = 333$–1000 RPS

The system response clearly changes frequency in each case. The time-varying long-period wobble in the system is caused by the sudden application of the input forces, which causes a slight misalignment between the angular momentum vector and the flywheel rotation axes. The system angular momentum vector gets larger as the flywheel speeds get further apart, giving the system as a whole more gyroscopic stiffness. The additional stiffness manifests in an increased oscillatory frequency and a smaller displacement from the equilibrium state as expected.

In all cases, the vibration-inducing imbalance forces are less significant than the system's slow oscillation. The magnitude of the imbalance-induced vibration is evidenced by the thickness of the lines seen in Figures 26–28. A closer look at the rotation of the support structure as shown in Figure 29 reveals that the wheel-synchronous vibration is small relative to the long-period oscillation. This figure shows the same data seen in Figure 26.

Adding a flexible appendage (representing a satellite structure such as an antenna or solar array) to the system does not change the response very much. Figure 30 shows the response of the system's flexible appendage, which has a natural frequency of 5 Hz. There is some vibration evident at the natural frequency of the appendage, but the response is dominated by the slow oscillation of the support structure.

The slow, changing oscillation seen in Figures 26–30 accurately reflects the response of a system with changing gyroscopic stiffness given an initial whirling type motion. The initial whirling motion seen in these figures, however, is an artifact of modeling, caused by the instant application of a disturbing force. Such a motion is possible and indeed uncontrollable in a two wheel IPACS, but it can only be caused by an external disturbance force. In an IPACS with full 3-axis control authority, the control in other dimensions would be used to eliminate the whirling motion.

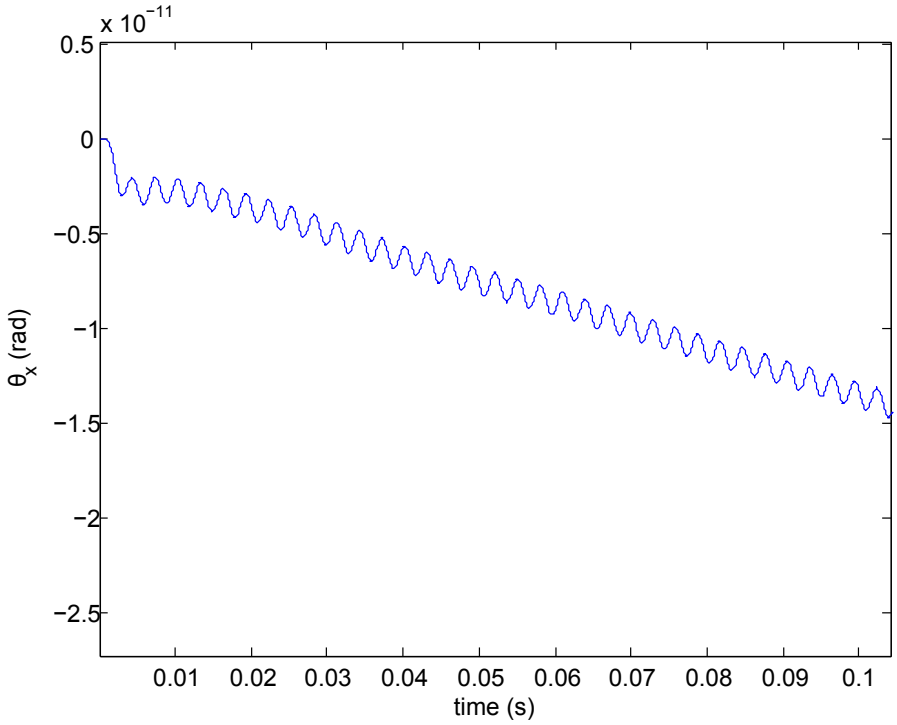

Figure 29: A closer look at the support structure vibration from Figure 26. This view shows the wheel-synchronous vibration

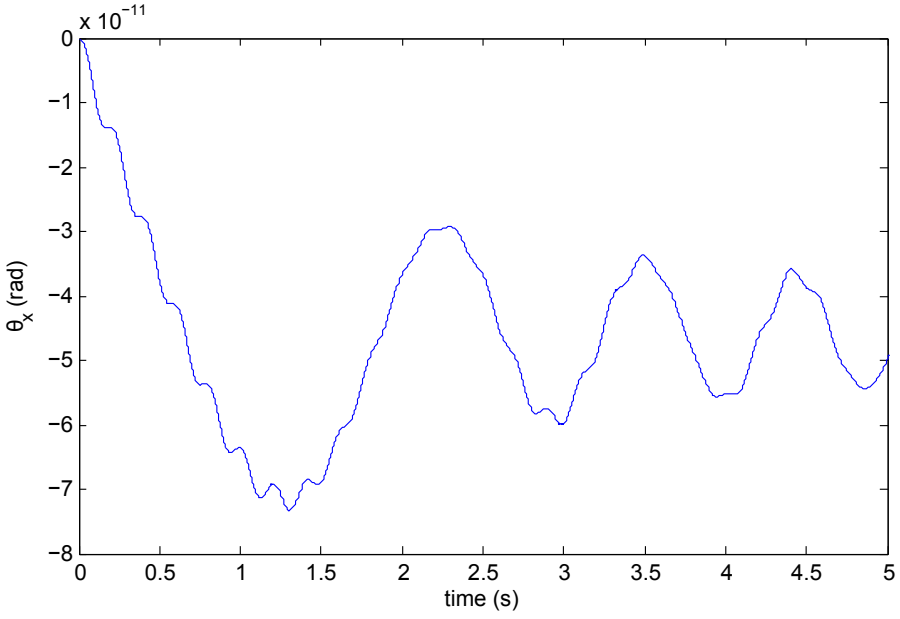

Figure 30: A closer look at the appendage vibration from Figure 26. This view reveals a small amount of vibration at the appendage's natural frequency, but behavior is dominated by long-period oscillation

4.2 Beat Frequency Analysis

After studying the effect of near-frequency input vibrations, it is evident that this model does not reveal any beat frequency problems. This is unsurprising given the linear nature of the model.

The flexible appendage *did* experience a small resonant vibration when the difference of two input frequencies matched the natural frequency of the appendage, but it experienced the same vibration with other unrelated input frequencies.

First, the two-wheel model was run with slightly different wheel speeds: 333 and 338 RPS. The 5 RPS difference in the wheel speeds creates a beat frequency which matches the natural frequency of the flexible appendage, which was not yet added. As Figure 31 shows, the 5 Hz beat frequency is clearly evident.

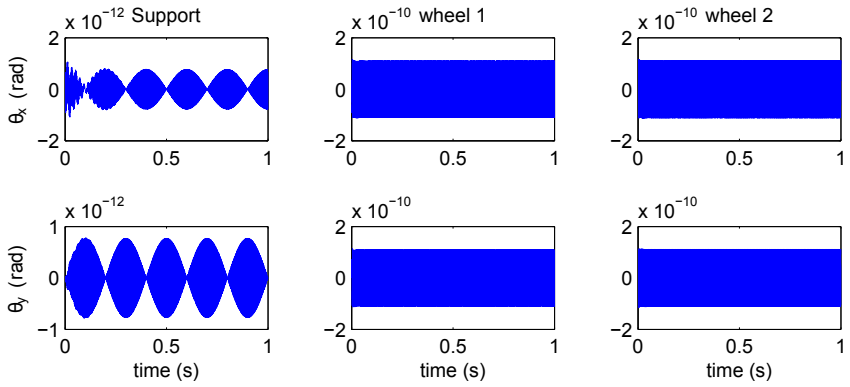

Figure 31: Beat frequency is clearly visible in the support structure when $\omega_1 = 333$, $\omega_2 = 338$ RPS

Next the model was run at the same wheel speeds with the flexible appendage added. The appendage represents a flexible satellite body such as a solar panel or antenna. The rotational state history from this test is shown in Figure 32. The beat frequency is still clearly visible, and the appendage is experiencing vibration near its natural frequency.

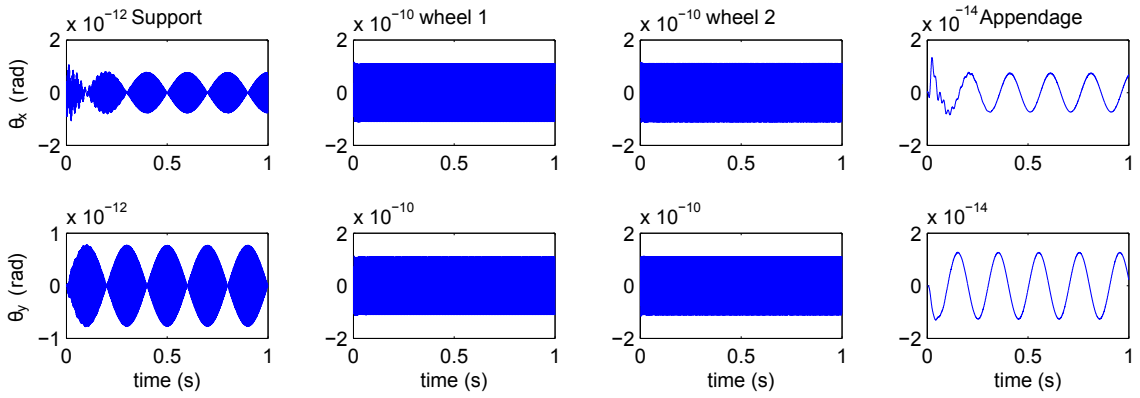

Figure 32: Beat frequency is still visible in the support structure when $\omega_1 = 333$, $\omega_2 = 338$ RPS, and the appendage experiences excitation at its resonant frequency of 5 Hz

Finally, the same model with flexible appendages was run with a new and wider wheel speed difference: $\omega_1 = 333$, $\omega_2 = 400$ RPS. This is shown in Figure 33. The beat frequency is no longer present, but the appendage still exhibits vibration near its natural frequency. The vibration magnitude of the appendage in this figure is largely the same as seen in Figure 32.

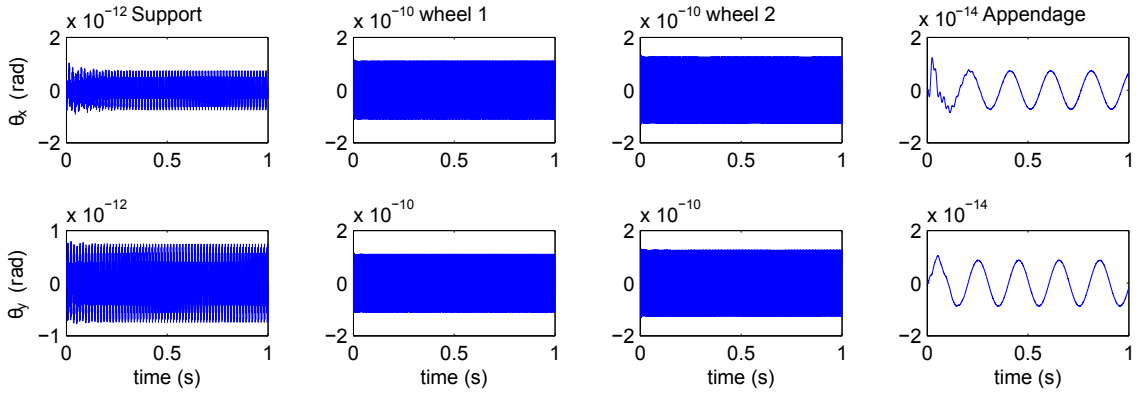

Figure 33: Beat frequency is gone, but appendage still vibrates near its resonant frequency of 5 Hz when $\omega_1 = 333$, $\omega_2 = 400$ RPS

From studying the results of the tests performed with both frequency offsets, it appears that there is no more low frequency excitation at the difference frequency of two inputs than there is at any other combination of inputs. The beat frequency

exists, but its effects are very limited. Recalling Equation 16, the combined output of two signals that are close in frequency can be written as

$$y = 2\sin\left(\omega_1 + \frac{\delta}{2}\right)t\cos\left(\frac{\delta}{2}\right)t$$

The maximum magnitude of the resultant vibrations shown in Figure 31 should be twice that of the vibrations evident when only one source of vibration is present. To check this, a test was run with only one wheel spinning. Figure 34 shows that the vibration magnitude is indeed approximately half of the peak seen when a beat frequency is present.

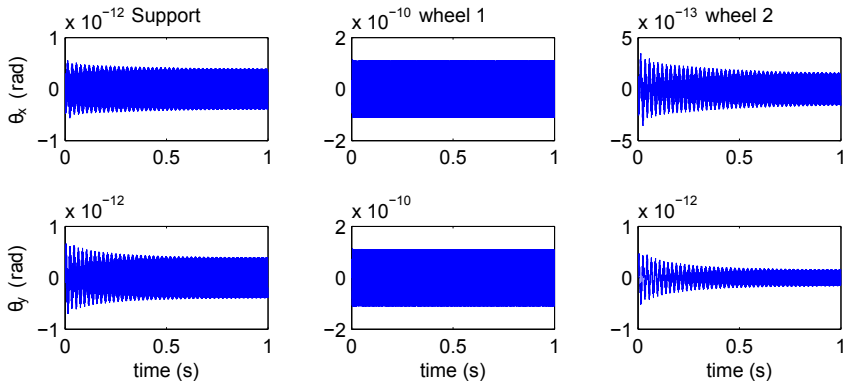

Figure 34: Vibration here, caused by one wheel rotating at 333 RPS, is approximately half the peak vibration seen in Figure 31

A power spectral density plot of the support structure's vibrations during beat frequency and non-beat frequency conditions reveals that there is no power at the low beat frequency. During the beat case, wheel speeds are: $\omega_1 = 333$, $\omega_2 = 338$ RPS. For the non-beat case, the speed of wheel 2 is raised to $\omega_2 = 400$ RPS. The peak-normalized PSD of both responses is shown in Figure 35.

The PSD reveals that there is no energy at the low beat frequency, and the rotation time histories reveal that there is no extraneous excitation as a result of the beat frequency. Aside from periodically doubling the magnitude of the resultant

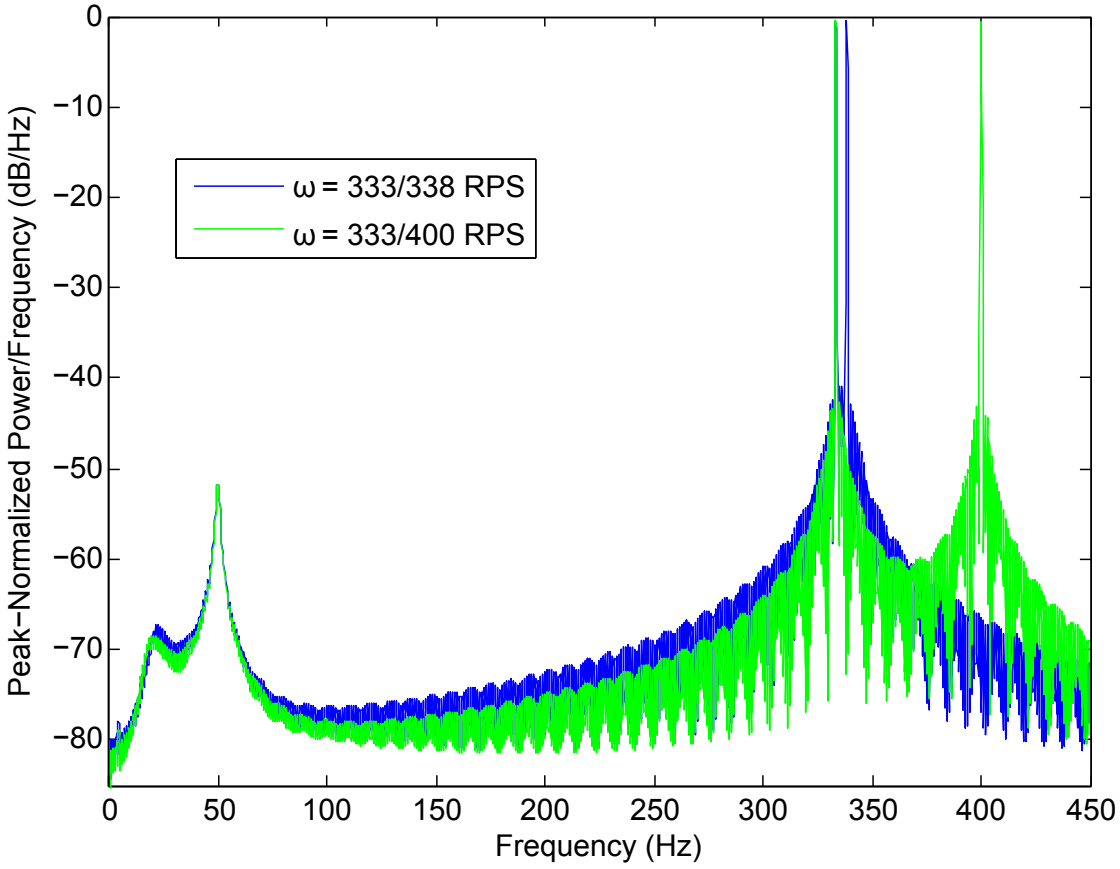

Figure 35: Peak-normalized PSD of support structure θ_x during beat ($\omega_1 = 333$, $\omega_2 = 338$ RPS) and non-beat ($\omega_1 = 333$, $\omega_2 = 400$ RPS) conditions. Low frequency response is nearly identical. Note peaks at the input excitation frequencies

high-frequency vibration, there is no negative effect from the beat phenomenon in a linear system.

4.3 Extra-Synchronous Whirl Excitation

Long rotors have a critical coning frequency, f_{con} where the wheel speed is synchronous with the forward whirl speed. This was illustrated with Figure 25 in Section 3.6.1. All rotors, however, have forward and backward whirl modes. With multiple flywheels in one system, the flywheels provide each other with extra-synchronous vibration sources, and it may be possible for these extra-synchronous frequencies to excite unexpected resonances. Both sub- and super-synchronous excitations were studied for this phenomenon.

In this section, ω refers to flywheel-specific wheel speed. Forward and backward whirl speed are respectively referred to as f_3 and f_4, which were derived and explained in Section 2.3.5. Spectrograms are used in this section to illustrate the time-varying nature of the response frequencies. All spectrograms are derived from θ_x (the rotation about x) of the wheel in question. Units are very small and are included only for the purpose of comparison between different cases. The satellite/support spring was used for all of the tests in this section.

4.3.1 Sub-Synchronous Whirl Excitation. A long-rotor model was used to look for sub-synchronous whirl excitation. Sub-synchronous resonance is vibration of a long rotor at speeds lower than the wheel speed. Sub-synchronous resonance is at a higher frequency than the critical coning frequency, f_{con}, where the forward whirl frequency crosses the wheel frequency. The region of interest using the flywheel parameters chosen for this study is seen in Figure 36, which shows both the forward and backward whirl of the long rotor used in this study.

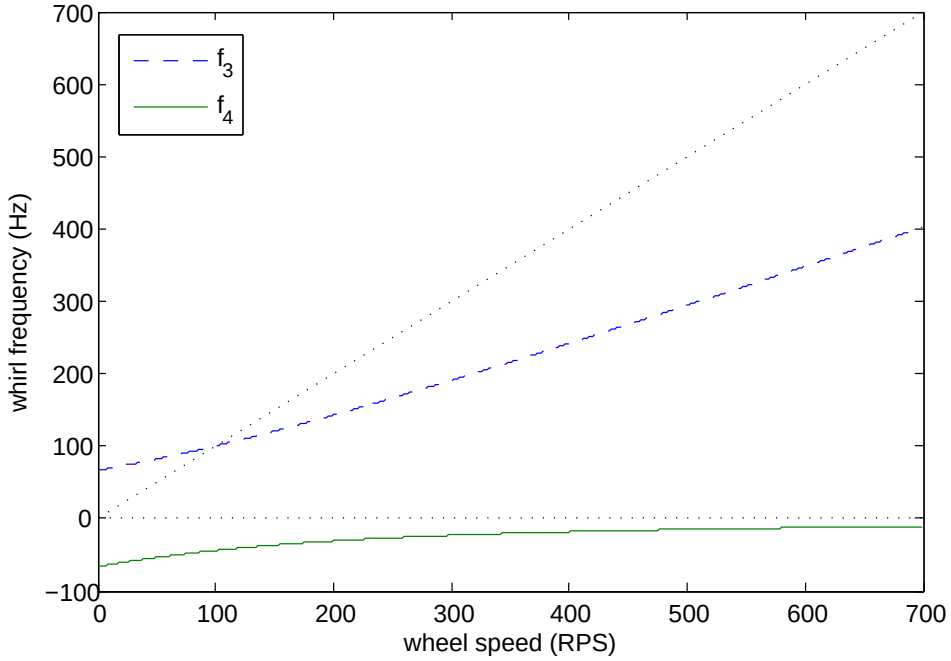

Figure 36: Forward and backward whirl modes of the sub-synchronous study model

In the sub-synchronous test, the wheels will spin at two different speeds. The vibration input of the slower wheel should excite a forward whirling mode in the faster wheel, even if the faster wheel is perfectly balanced.

The flywheel parameters used for this study are shown in Table 5. Other parameters remain the same as those shown in Table 1 from Section 3.2.3. This model was studied both with and without bearing damping included. These values were chosen not for realism, but to give favorable conditions for excited whirl at a frequency other than the wheel frequency.

Table 5: Flywheel parameters for sub-synchronous study

mass	m	10	kg
polar MOI	I_P	0.1125	kg-m^2
transverse MOI	I_T	0.2015	kg-m^2
rotor MOI ratio	P	0.5583	

In the sub-synchronous test, wheel 2 was perfectly balanced and operated at 700 RPS. This gives it a forward whirl frequency of $f_3 \approx 400$ Hz and a backward whirl frequency of $f_4 \approx -11$ Hz. Wheel 1 was given a moment-inducing imbalance and operated at speeds intended to excite f_3 of the faster balanced wheel, or about 400 RPS. Wheel 1's own speed, ω_1 caused separate whirling frequencies in wheel 1: $f_3 \approx 242$ Hz and $f_4 \approx -18$ Hz. Natural frequencies can be found by inspection from Figure 36 and analytically with Equations 12 and 13 from Section 3.2.3. In all cases the speed of wheel 1 (the unbalanced excitation wheel) varies from 350 RPS at $t = 0$ to 450 RPS at $t = 2$.

4.3.1.1 Undamped sub-synchronous response. At first, damping was neglected to see if there would be any response. Wheel 1's response is shown in Figure 37. Note the strength of the self-induced, sub-synchronous, forward whirling mode. This wheel is well past its critical coning speed for forward whirl, but it is still responding strongly at the whirling frequency. In fact, at lower wheel speeds the resonant forward whirling response is *stronger* than the input disturbance.

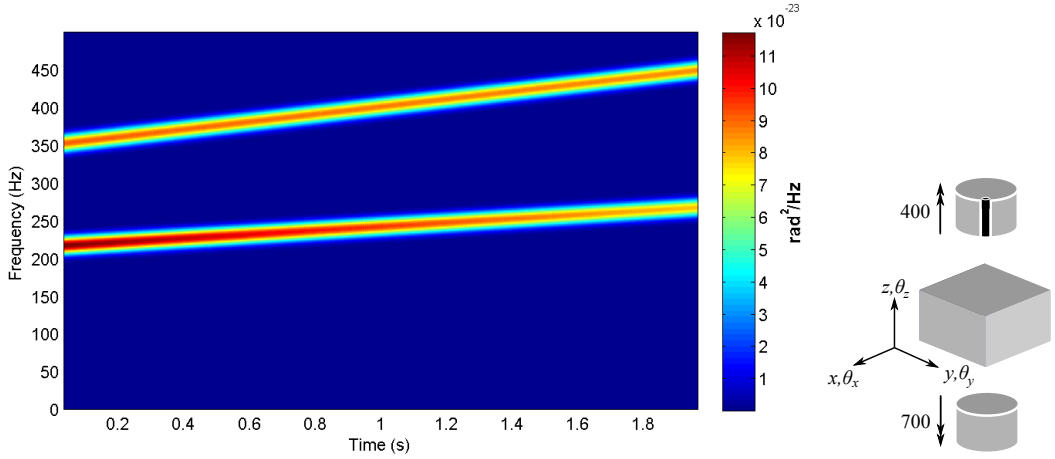

Figure 37: Spectrogram of wheel 1's response to its own undamped imbalance. ω_1 varies from 350–450 RPS. Note the strong forward whirling resonance

Wheel 2's response over the same time period was examined at multiple speeds. Figure 38 shows the wheel 1 response at a baseline of $\omega_1 = 0$ and at $\omega = \mp 700$ RPS. Wheel 2 experienced a significant forward whirling motion when it was rotating in the same direction as wheel 1. Support response in all cases was similar.

Two spurious vibrations can be found in Figure 38. Most notable is the constant frequency vibration at approximately 50 Hz which appears in 38(a) and 38(c). The 50 Hz vibration appears to be worse when the excitation is at 400 Hz, but it is actually worse at approximately 1 sec, and occurs repeatedly if the integration time is longer. There is also a vibration at approximately 70 Hz visible in 38(a). These vibrations do not match either of the rotor's resonant frequencies, and they are system level effects caused by the bus/support springs and the net gyroscopic stiffness.

Two notable vibrations do appear, however. The first of these vibrations is at the backward whirl frequency, f_4, of wheel 1 (the excitation wheel). This vibration at approximately 20 Hz is visible in all three scenarios of Figure 38, but is strongest in the response shown in Figure 38(c), which is the case where the wheels are spinning in opposite directions. This excitation indicates that wheel 1 is exciting its own backward whirl mode through interaction with wheel 2, *even though wheel 2 is perfectly balanced.*

The other vibration apparent in Figure 38 is the vibration that appears near $t = 1$ second at approximately 400 Hz in 38(b). This frequency is the forward whirl speed of wheel 2, and the intended excitation frequency of this test model. This vibration appears and is most severe about halfway through the test, when the excitation frequency is 400 Hz. Forward whirl in wheel 2 is expected to be worst at that time because it is being excited at f_3. The persistence of the whirling motion after the excitation frequency has moved past the resonant frequency shows that whirl tends to persist after excitation. The same time history appeared when wheel 1's speed was

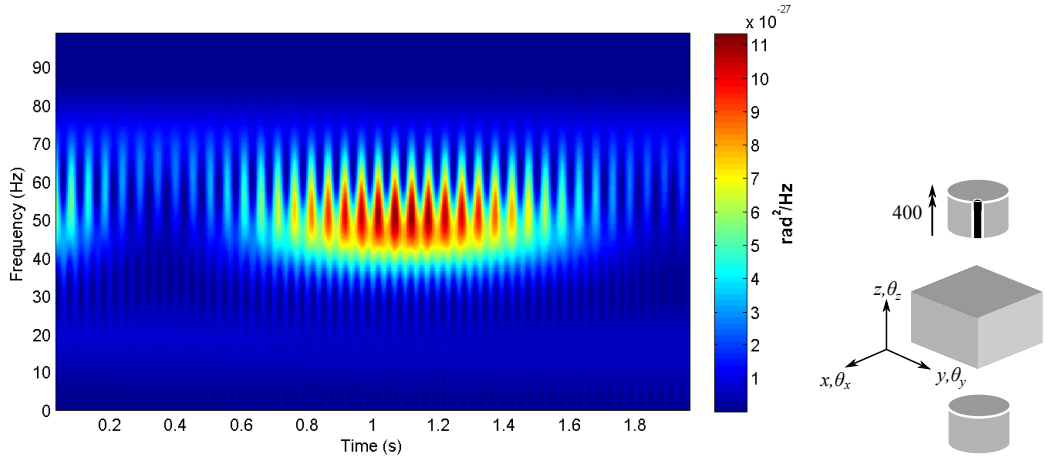

(a) $\omega_2 = 0$

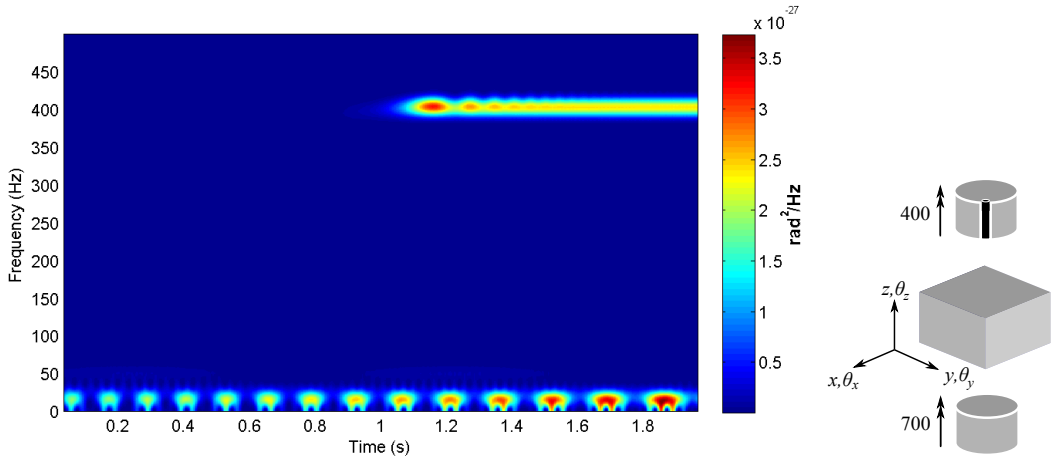

(b) ω_2 = -700 RPS

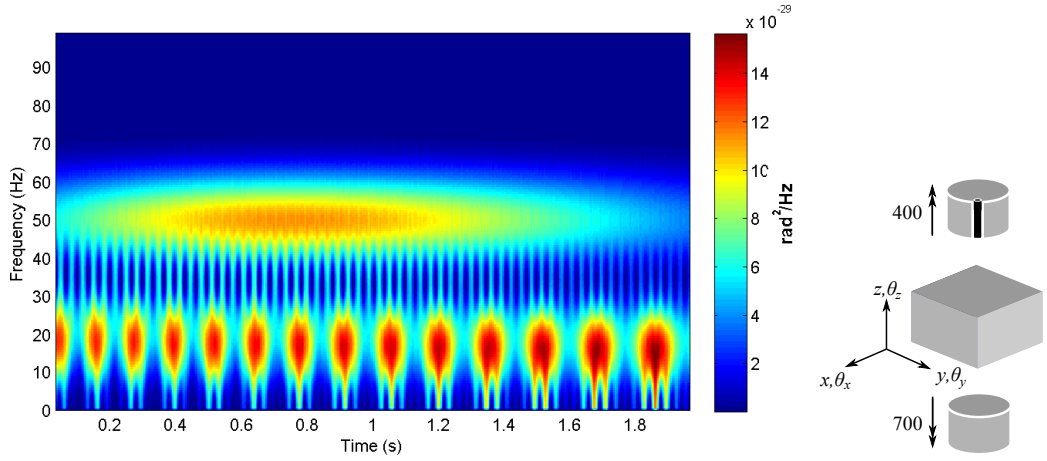

(c) ω_2 = 700 RPS

Figure 38: Spectrogram of wheel 2's response to sub-synchronous vibration input. ω_1 varies from 350–450 RPS. Note the different frequency scale in subfigure (b). Vibration at 50 Hz fades in and out repeatedly

varied backwards, from 450–350 RPS. In other words, the appearance and decrescendo of a whirling motion was consistent in time, not in input frequency.

Note that the model configuration represented in 38(b) is not operationally realistic for a two wheel IPACS, but it demonstrates sub-synchronous excitation. The problem is that both wheels are spinning in the same direction, which does not allow for high power storage and transfer with a net zero angular momentum change. In reality, the wheels will be spinning in opposite directions as they are for the case shown in Figure 38(c). This situation might occur, however, in a bank of multiple rotors, such as one being used primarily for energy storage.

4.3.1.2 Damped sub-synchronous response. Since sub-synchronous excitation was found to affect a two flywheel system with no damping, the next step was to see if it remained when damping was included in the model. The same test conditions used in the undamped case were used to study a more realistic damped flywheel configuration.

Figure 39 shows the response of wheel 1, the excitation wheel. Note that the resonant whirling response has been attenuated below the threshold of visibility in this spectrogram and all that remains is the synchronous imbalance-induced vibration. Since the wheel speed is so far from the critical whirling frequency f_{con}, even the very small amount of damping present in this model is enough to eliminate this resonance.

Figure 40 shows the damped response of wheel 2 to the same sub-synchronous imbalance input that induced forward and backward whirl in the undamped case. All resonances have fallen below the detectable threshold, leaving only the direct input frequency created by the unbalanced rotation of wheel 1.

From the significant and beneficial effect of even modest damping in this multiple flywheel IPACS model, it appears that real flywheel systems are safe from the harmful

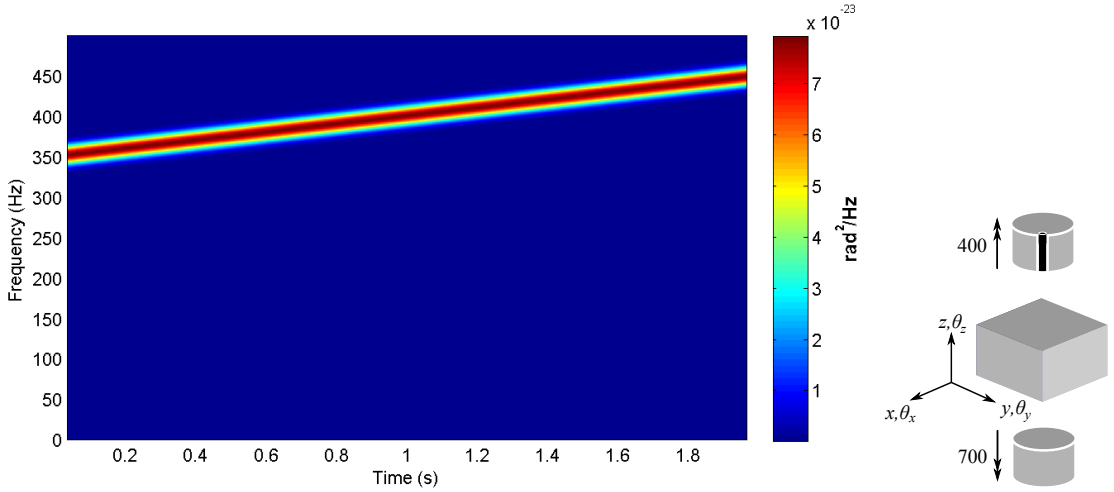

Figure 39: Spectrogram of wheel 1's response to its own damped imbalance. ω_1 varies from 350–450 RPS. The forward whirling resonance is gone

effects of sub-synchronous flywheel vibration in an axially opposed configuration. Real flywheels necessarily include damping since it is a real and unavoidable physical phenomenon.

4.3.2 Super-synchronous Whirl Excitation. A short-rotor model with the nominal parameters given in Table 1 from Section 3.2.3 was used to look for super-synchronous whirl excitation. Super-synchronous resonance is vibration of a short rotor at speeds higher than the wheel speed. Ordinarily this is not a problem for short rotors, since their forward whirling frequencies always remain higher than the wheel speed. An external vibration input at the resonant speed could induce vibration in this mode, however. Figure 41 shows the forward and backward whirling frequencies, f_3 and f_4, for this configuration.

This test used the same setup as the test for sub-synchronous whirl, with different rotors and a different excitation speed. In this test wheel 1 was spun from 950–1050 RPS in an attempt to excite vibration modes in wheel 2, which was spinning at $\mp$700 RPS. A non-spinning wheel was again used as a baseline. Whirl modes

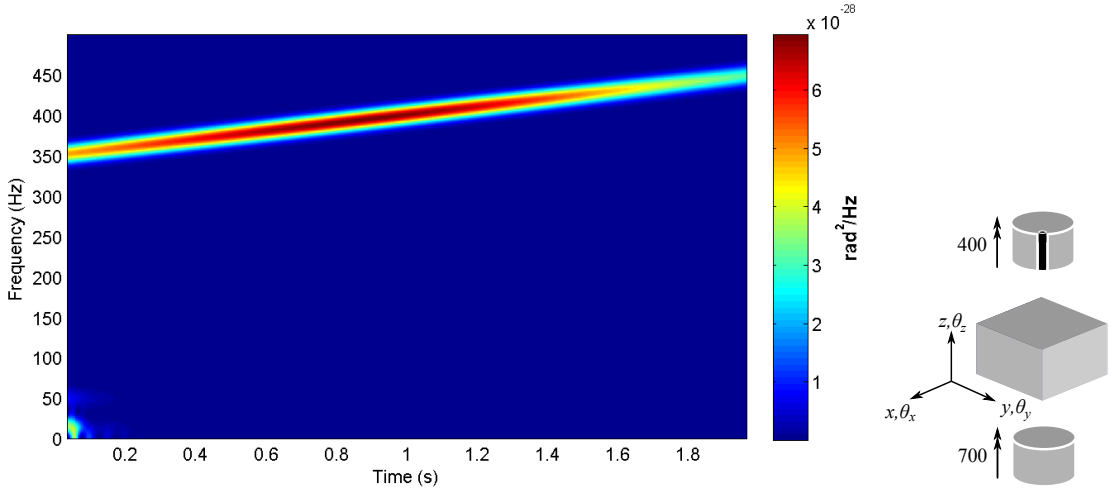

(a) ω_2 = -700 RPS

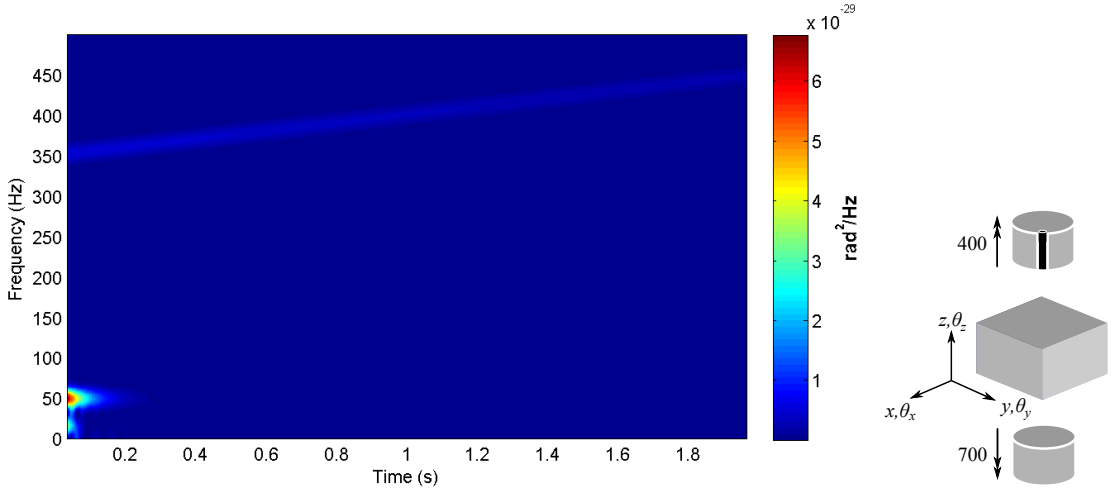

(b) ω_2 = 700 RPS

Figure 40: Wheel 2 damped sub-synchronous spectrograms. ω_1 varies in time from 350–450 RPS. Frequencies other than the input have been attenuated

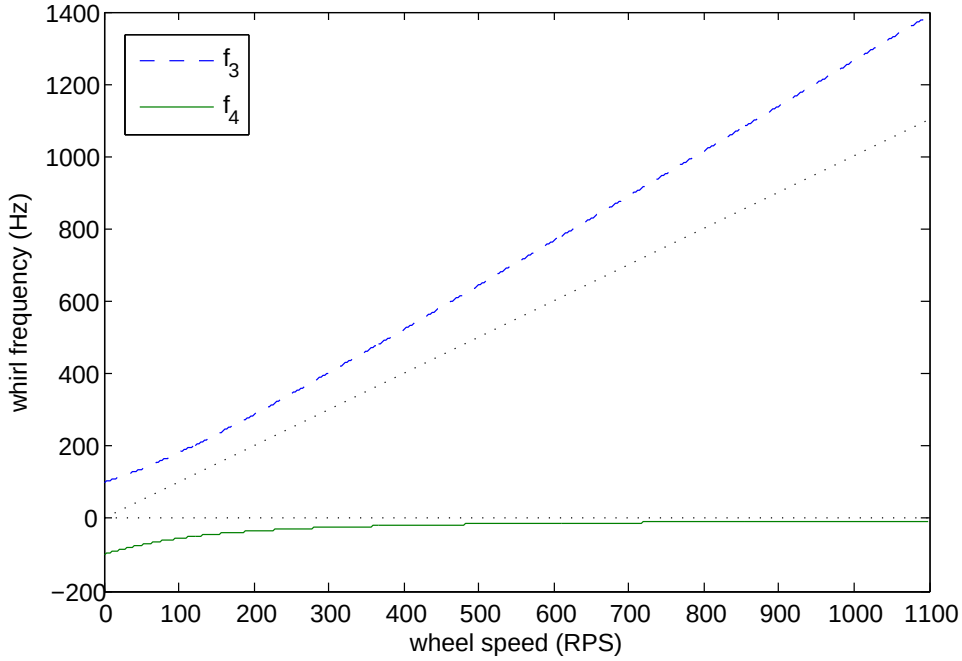

Figure 41: Forward and backward whirl modes of the super-synchronous study model. One dotted line is zero and the other is synchronous with the wheel speed.

for wheel 2 are $f_3 \approx 890$ Hz and $f_4 \approx -12$ Hz. For wheel 1, $f_4 \approx -7.9$ Hz. f_3 for wheel 1 is well above any vibrations present in the system, since the rotors are short.

Damping was again at first neglected to see if there would be a response. The super-synchronous excitation response was very similar to the sub-synchronous excitation response. Spectrograms in this section show a wheel 1 speed range from 850 RPS at $t = 0$ to 950 RPS at $t = 2$.

Spectrograms of the wheel 1 and support responses did not reveal any resonances. The only place in the model with any visible extra-synchronous frequency response was wheel 2. The spectrograms for wheel 2 are shown in Figure 42. Similar to the sub-synchronous case, there is a slight forward whirl response when spin directions are identical, and there is a slight backward whirl excitation regardless of relative spin directions.

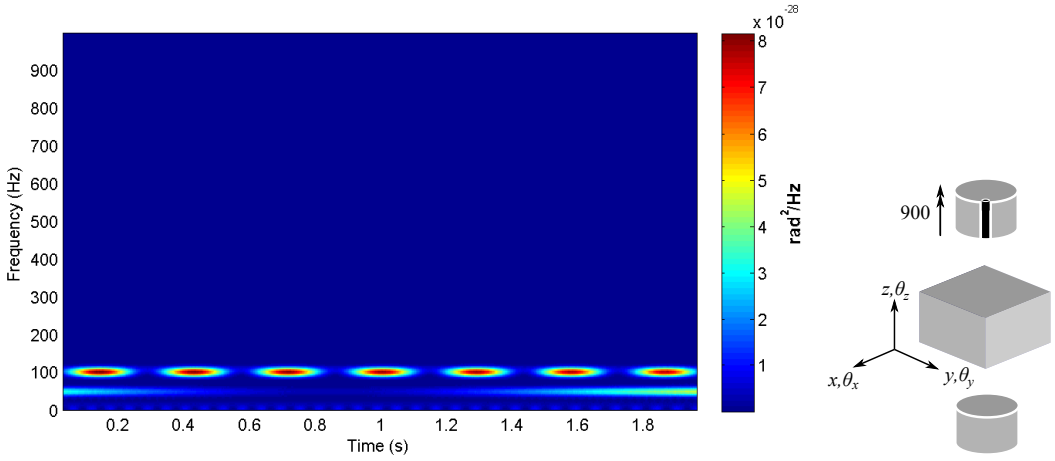

(a) $\omega_2 = 0$

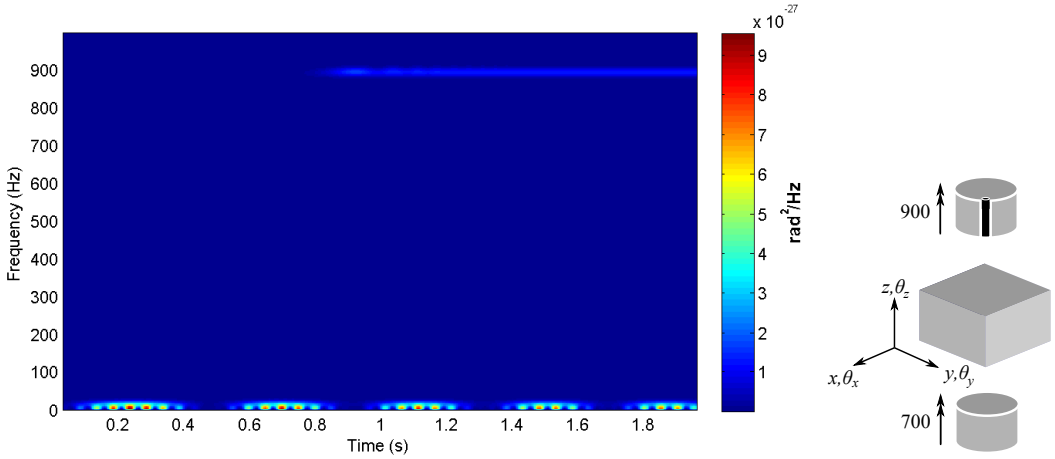

(b) ω_2 = -700 RPS

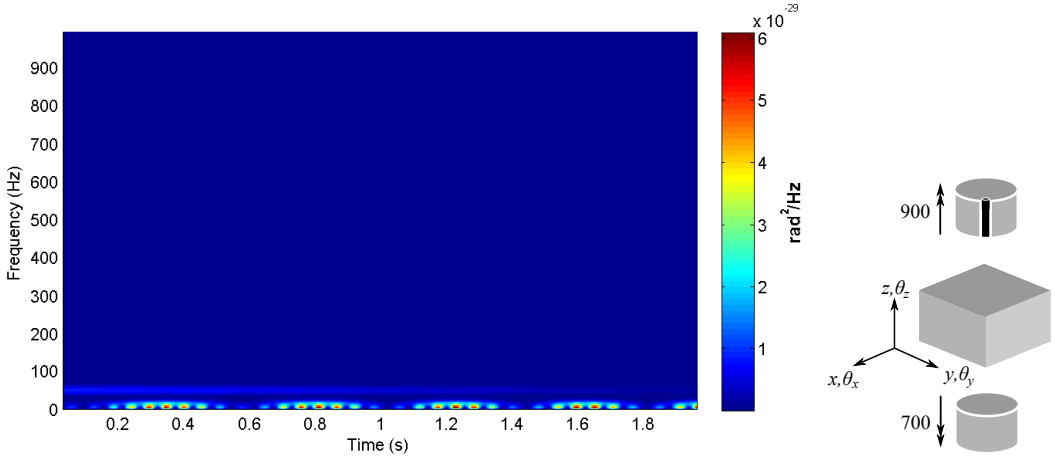

(c) ω_2 = 700 RPS

Figure 42: Spectrograms of wheel 2's undamped response to super-synchronous vibration input. ω_1 varies in time from 850–950 RPS

Figure 42 also reveals a slight response around the backward whirl modes. There is not enough spectral resolution in the figures to determine which wheel's response is causing the vibration. They are very close in frequency, however (approximately 8 and 12 Hz), and perhaps both of them are responding.

As seen in Figure 43, resonant vibrations due to a super-synchronous vibration excitation disappear when damping is included in the model, similar to the disappearance of resonant vibration in the sub-synchronous test.

4.4 Summary

The model developed in this thesis was used to investigate potential causes of troublesome low frequency vibration in an IPACS. Beat frequency was found to have absolutely no impact on low frequency vibrations, and minimal impact at any frequency, with the only impact being the periodic doubling of the input forces. Extra-synchronous resonance excitation, both sub- and super-synchronous, was found to have only a small impact on satellite vibrations. Backward whirl was excited regardless of spin directions, but extra-synchronous forward whirl was only excited when spin directions were identical. Extra-synchronous vibration is *very* small relative to the inducing imbalance, but it is at a lower frequency. The identical spin direction configuration is of no concern for a simple IPACS, but could be a factor in a bank of flywheels intended primarily for energy storage. With a small amount of damping, however, all extra-synchronous vibration effects disappear.

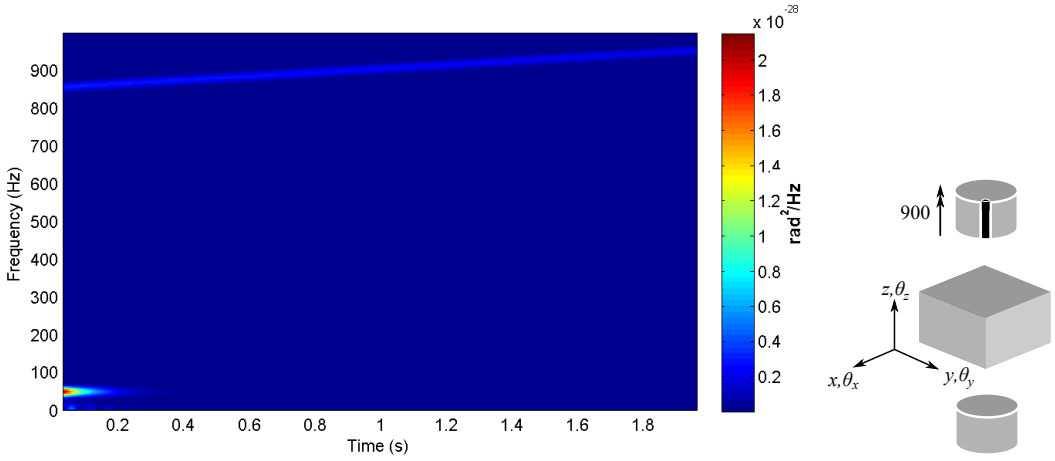

(a) $\omega_2 = 0$

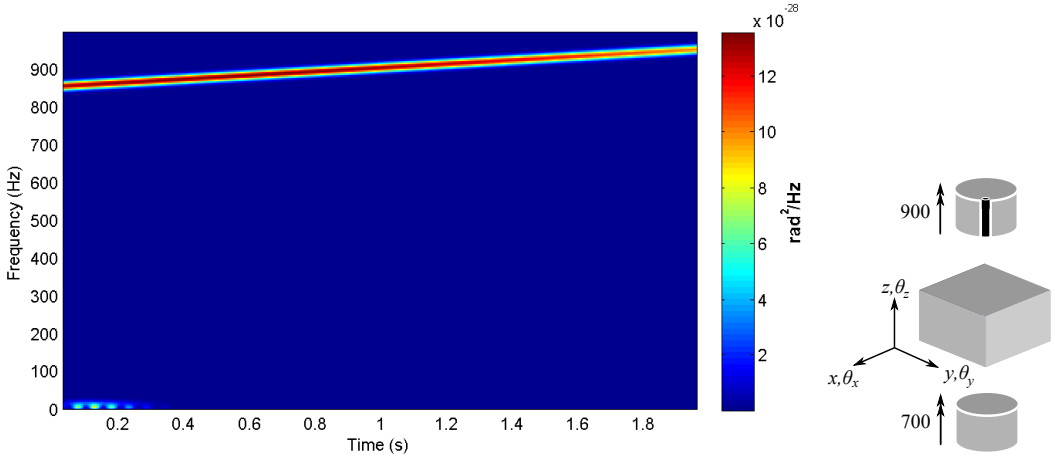

(b) ω_2 = -700 RPS

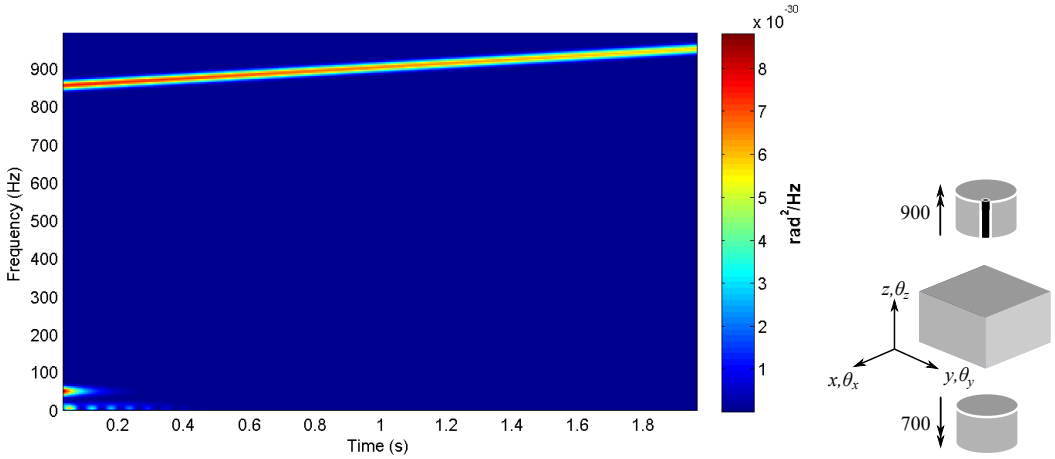

(c) ω_2 = 700 RPS

Figure 43: Spectrograms of wheel 2's damped response to super-synchronous vibration input. ω_1 varies in time from 850–950 RPS

V. Conclusion

5.1 Summary

In this thesis a flexible linear dynamics model was developed to study vibrations in a system of multiple connected gyroscopic flywheels. The model was validated through several types of test input, and then used to analyze various sources of vibration interaction between two flywheels a simulated IPACS. System parameters were intended to be representative of a near-future technology demonstration mission to validate the use of flywheels for energy storage and attitude control in space.

The source of vibration studied in this model was an assumed eccentricity caused by manufacturing defect. Furthermore, it was assumed that this defect was attenuated by active magnetic bearing control methods described in previous literature. The residual vibrations after attenuation were used as model inputs. The vibration inputs were applied in the radial and transverse directions to an axially-aligned two-flywheel IPACS.

The model was then used to study interactions between multiple sources of vibration in an IPACS. Specifically, the beat frequency and extra-synchronous vibration excitation phenomena were studied, including both sub- and super-synchronous vibration excitation scenarios.

5.2 Findings

The beat frequency problem was shown to have almost no impact in a linear system. The extra-synchronous vibration effects were both found to have a small effect on a double flywheel system. When mild damping was applied, effects were below the threshold of observability, but with no damping there was a small but consistent system response to backward whirl modes. In addition, if there are multiple flywheels

with the same spin direction, extra-synchronous forward whirl in one wheel can be excited by another unbalanced wheel.

Of the vibration sources considered in this thesis, extra-synchronous resonance excitation, both sub- and super-synchronous, proved to be of some potential concern in the future development of IPACS. As bearing and flywheel system technology continues to improve, damping will continue to fall as flywheel designers seek to remove sources of loss from their systems. At some point the damping may be small enough to allow the extra-synchronous resonances to affect the system negatively. Vibrations caused by input interactions are *much* smaller than the vibrations themselves, but they are also at a lower frequency.

Park proposed a notch filter centered at the wheel speed to mitigate the effects of wheel imbalance to an IPACS or satellite. If bearing development produces magnetic bearings with low enough damping to allow the extra-synchronous resonant vibration to become a problem, the control system designer could also develop methods for mitigating extra-synchronous vibration modes.

5.3 Contributions

This thesis proved the existence of inter-flywheel vibration interactions in a multiple flywheel system. Extra-synchronous resonance excitation between multiple rotors was found to exist in an ideal undamped configuration, but even a very small realistic amount of damping was enough to mitigate the effect to the point that it was less of a concern than individual rotor vibration inputs.

5.4 Recommendations for Future Work

This thesis showed that damping can mitigate and possibly eliminate undesirable extra-synchronous flywheel vibration. Future research should be done to de-

termine how low the bearing damping can be before the sub-synchronous resonance negatively affects system operation.

In addition, the model developed in this thesis was used to investigate some of the effects of multiple flywheel vibrations in an IPACS, but this thesis was limited in scope to analyzing two co-axial rotors with simple imbalance-induced vibrations in and about 2 axes. In an advanced flywheel there is also significant potential for rotational vibration about the spin axis due to torque ripple. In the co-axial case the torsional vibrations will remain independent from other system disturbances, but in a flywheel system with multiple non-co-axial rotors, torsional vibrations will induce other vibrations that may be deleterious to successful IPACS implementation on a satellite.

The analysis of those extra factors should be undertaken as a further step along the path to developing flywheel energy storage systems. With torsional stiffness turned on and the appropriate input forces applied, the model developed in this thesis is capable of performing this evaluation.

Furthermore, as flywheel performance continues to improve and bearing development produces magnetic bearings with lower losses, the vibration interaction effects uncovered in this thesis may become significant. If that occurs, flywheel bearing controllers must be able to account for and mitigate the effects of backward whirl excitation between flywheels.

5.5 Conclusion

Flywheels may someday be a key component for providing the satellite designer with flexibility and performance benefits. Their successful on-orbit deployment has to this point been delayed longer than any of the original proponents of the idea could have envisioned, and many problems in this area remain unstudied. Someday,

however, enough problems will be solved to make flywheels in orbit a viable reality. The engineering community must continue to work diligently in this area until that day arrives.

Appendix A. One Integration Problem and a Solution

Position is the double integration of acceleration, which is proportional to the input force as shown in Equation 29.

$$x(t) = \int v(t) = \iint a(t) = \iint \frac{f(t)}{m} \tag{29}$$

Given sinusoidal inputs acting on a 1 kg mass:

$f(t) =$	$\sin t$	$\cos t$
$a(t) =$	$\sin t$	$\cos t$
$v(t) =$	$-\cos t + c_1$	$\sin t + c_1$
$x(t) =$	$-\sin t + c_1 t + c_2$	$-\cos t + c_1 t + c_2$

If the mass is initially at rest ($x_0 = v_0 = a_0 = 0$), the constants are found to be:

$f(t) =$	$\sin t$	$\cos t$
$c_1 =$	1	0
$c_2 =$	0	1

When a sine wave force is applied to an unconstrained mass initially at rest, c_1 will cause a positive secular drift. This drift does not occur if the input force is a cosine wave. The difference between sine and cosine input forces is illustrated in Figure 44.

The drift illustrated in Figure 44 is a phenomenon observed only in modeling; it does not occur in real systems. Most models do not reveal the drift because they model systems constrained by some spring force. For unconstrained systems, a model can reveal a drift, but it does not exist in reality because the periodic rotating forces

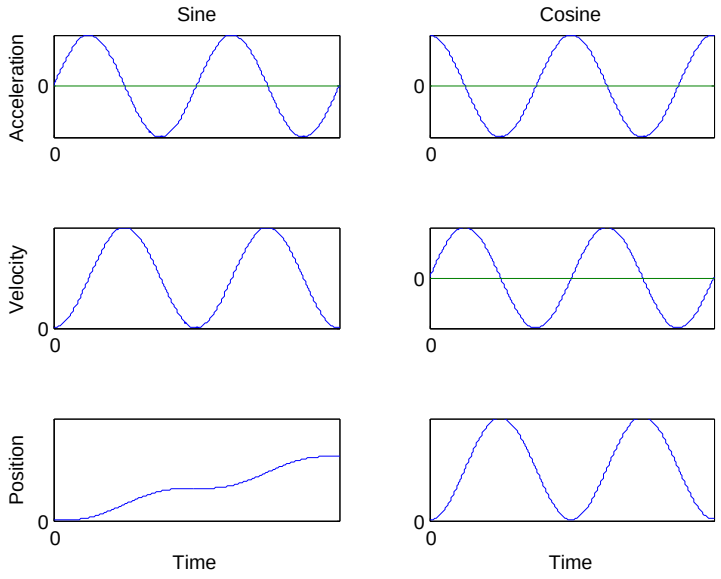

Figure 44: Acceleration, velocity, and position due to sinusoidal inputs applied to a free body initially at rest

such as wheel imbalances always grow from an initial magnitude of zero. It is only a factor when modeling a system that is rotating at $t = 0$.

Because the rotating force must be represented as a sine wave in one dimension, the direct application of this force will cause a secular drift. One solution is to delay the application of this force until the input force has rotated 90°. This delay will cause the sine wave to look like a cosine wave (it will begin from 1 rather than from 0), and it will be shifted correctly in phase. With multiple input forces, each one must be "turned on" at the appropriate moment. Given the numerical nature of the model in this thesis, the limits of integration must match these times as well to ensure that the sine input is applied at exactly the right moment. "Turning on" the forces at the correct times will eliminate this source of drift.

Listing B.1: ../models/model.m

```
function [output] = model (config)
global ss model input output c ii model
% Feb 2011
% Jordan Firth

% state = [x y z a b g x' y' z' a' b' g']'

%% constants
% compute/import data from case_maker
[model,input] = case_reader(config);

%% R Matrices
% r3- each page of array is rot mat for one wheel
% r12- blkdiag of 4 r*3's- rotate all 4 states of the wheel at once

% R- one giant rotation matrix for the whole massive A matrix-may not need

% Here are the rz's
r3 = zeros(3,3,model.nwheels); % preallocate for speed
r12 = zeros(12,12,model.nwheels); % preallocate for speed
R = zeros(model.nwheels*12); % preallocate for speed
for i = 1:model.nwheels
    r3(:,:,i) = Rmaker1(model.zps(:,i)); % r3 is ind. rot. matrix
    %blkdiagn creates super-duper 4x rot. matrix (x..a..dx..da..)
    r12(:,:,i) = blkdiagn(r3(:,:,i),4); % stores all r12's in array
    R(12*i-11:12*i, 12*i-11:12*i) = r12(:,:,i); % giant rotation matrix
end

%% mi's- mass matrix inverses

% compute M inverses once and store for speed
mbusi6 = model.msupport^-1;

mi6 = model.mwheel^-1;
mi12 = blkdiag(eye(6), mi6);

% mi for dummy mass
if model.dummy
        mdummyi6 = model.mdummy^-1;
end

%% A Matrix
% Create a-matrices and assemble into A

ss.A_rb = blkdiagn([zeros(6) eye(6); zeros(6,12)],model.nwheels);

% % these are useful sometimes when the model breaks
% size(rz12(:,:,1))
% size(blkdiag(Mbusi6,Mi6))
% size(k)

% K and C terms
for i = 2:model.nwheels

    % K
    K = r12(:,:,i) * blkdiag(mbusi6,mi6) * model.k * r12(:,:,i)';
    ss.A_rb(7:12,1:6) = ss.A_rb(7:12,1:6) + K(1:6,1:6);
    ss.A_rb(7:12,12*i-11:12*i-6) = ss.A_rb(7:12,12*i-11:12*i-6) + K(1:6,7:12);
    ss.A_rb(12*i-5:12*i,1:6) = ss.A_rb(12*i-5:12*i,1:6) + K(7:12,1:6);
    ss.A_rb(12*i-5:12*i,12*i-11:12*i-6) = ss.A_rb(12*i-5:12*i,12*i-11:12*i-6) + ...
        K(7:12,7:12);

    % C
```

```
64      C = r12(:,:,i) * blkdiag(mbusi6,mi6) * model.c * r12(:,:,i)';
65      ss.A_rb(7:12,7:12) = ss.A_rb(7:12,7:12) + C(1:6,1:6);
66      ss.A_rb(7:12,12*i-5:12*i) = ss.A_rb(7:12,12*i-5:12*i) + C(1:6,7:12);
67      ss.A_rb(12*i-5:12*i,7:12) = ss.A_rb(12*i-5:12*i,7:12) + C(7:12,1:6);
68      ss.A_rb(12*i-5:12*i,12*i-5:12*i) = ss.A_rb(12*i-5:12*i,12*i-5:12*i) + ...
69          C(7:12,7:12);
70  end
71
72  ss.A_rb(7:12,1:6) = ss.A_rb(7:12,1:6) + mbusi6 * model.busk;
73
74  % here is my dummy mass for vibe
75  if model.dummy
76          x=model.nwheels*12+1;
77          a = [zeros(6) eye(6) ; mdummyi6*model.kdummy(7:12,7:12) zeros(6)];
78          ss.A_rb = blkdiag(ss.A_rb,a);
79
80          ss.A_rb(7:12,1:6) = ss.A_rb(7:12,1:6) + mbusi6*model.kdummy(1:6,1:6);
81          ss.A_rb(7:12,x:x+5) = ss.A_rb(7:12,x:x+5) + mbusi6*model.kdummy(1:6,7:12);
82          ss.A_rb(x+6:x+11,1:6) =ss.A_rb(x+6:x+11,1:6) + mdummyi6*model.kdummy(7:12,1:6);
83          clear a
84
85  input.q0 = [input.q0; zeros(12,1)];
86  end
87
88  %% B Matrix
89
90  ss.B = zeros(12*model.nwheels,model.nwheels); % preallocate for speed
91  clear a
92  for ii = 2:model.nwheels;
93      a = zeros(12,2);
94      a([7 10],1) = input.b([7 10],ii);
95      a([8 11],2) = input.b([8 11],ii);
96
97          ss.B(12*ii-11:12*ii,2*ii-1:2*ii) =  r12(:,:,ii) * mi12 * a;
98  end
99  clear a
100
101 % input.b1 creates constant direction input forces (just for testing)
102 input.b1 = mi12*input.b1;
103 input.b1 = input.b1(:);
104 ss.B = [ss.B input.b1];
105
106 %% W matrices
107 % these will actually be created in the solver, but I do as much work here
108 % as possible to save integration time
109
110 % W
111 % stretch vector: mathworks.com/matlabcentral/newsreader/view_thread/129069
112
113 input.w_(1,:) = input.w(1,:);
114 input.w_(2,:) = (input.w(2,:)-input.w(1,:))/(input.time);
115
116 a = repmat(input.w_(1,:),12,1);
117 b = repmat(input.w_(2,:),12,1);
118
119 % input.w_ = input.w_';
120
121 input.W(:,:,1) = diag(a(:));
122 input.W(:,:,2) = diag(b(:));
123 clear a b
124
125 %% G matrices
126 % these will actually be created in the solver, but I do as much work here
127 % as possible to save integration time
128 Ip = model.mwheel(6,6);
129 ss.G = zeros(12*model.nwheels);
```

```
for i = 2:model.nwheels
    j = 12*i;
    ss.G(j-2:j,j-2:j) = Ip * r3(:,:,i) * mi6(4:6,4:6) * ...
        [[0 -1 0];[1 0 0];[0 0 0]] * r3(:,:,i)';
end

%% find integration times
% Each wheel must be integrated to and from the time when it crosses
% theta = pi/2. Here I find those times and create a time vector which
% contains the appropriate integration limits.

clear a b
a = [input.w_(2,:)/2; input.w_(1,:); -pi/2*ones(1,model.nwheels)]';
b=[];
for ii = 1:model.nwheels
    b = [b roots(a(ii,:))']; % only need the max time
end

% remove solutions outside of my time window (0-tf)
b=b(b>0);
b=b(b<input.time);

t = unique([0 b input.time]); % [0, intermediate times, tf]

clear a b

%% fix matrices for dummy mass
if model.dummy
        ss.B = [ss.B; zeros(12,size(ss.B,2))];
        ss.G = blkdiag(ss.G,zeros(12));
        x = model.nwheels*12;
        input.W = cat(2,input.W,zeros(x,12,2));
        input.W = cat(1,input.W,zeros(12,x+12,2));
        clear x
end

%% solve equation
% run with state_space_model (no need to run the entire model 10000 times)

options = model.options;
output.t = [];
output.q = [];
for ii = 1:length(t) - 1
    time = [t(ii) t(ii+1)-1E-80];
[output_t,output_q] = ode45(@state_space_model,time,input.q0,options,input,ss);
output.t = [output.t; output_t];
output.q = [output.q; output_q];

input.q0 = output.q(size(output.q,1),:);
end;

end

function dq = state_space_model(t,q,input,ss )
% global A q B u
% global peanut teakettle
% W(t) varies from w0 to wf- used to get correct gyro stiffness in A
W = input.W(:,:,1) + input.W(:,:,2) * t;


% vibe input has to look like a cosine (start from 1). If it looks like a
% sine, the position drifts. Since the circular force of the imbalance
% needs both sines and cosines, I have to include sines, but I accomplish
% it by not starting them until theta = pi/2

% this is where i determine theta
```

```
theta = (input.w_(1,:)*t + input.w_(2,:)/2*t^2);

% here is wheel speed at t=time
w = (input.w_(1,:) + input.w_(2,:)*t);
% peanut = [peanut w(2)]; see w while testing
% teakettle = [teakettle t]; see t while testing- to match up with w

% this is the magnitude of the centripetal force input
u_mag = input.e * w.^2;

% and here I test and only include the sine if theta>=pi/2
% sin/cos(theta) is direction; u_mag is magnitude
u = [cos(theta).*u_mag; sin(theta).*u_mag.*(abs(theta)>=pi/2)];

u = [u(:); 1];

B = ss.B;

A = ss.A_rb + W*ss.G;

dq = A*q + B*u;
end
```

Listing B.2: ../models/case_reader.m

```
function varargout = case_reader(file_num)
% clc;
% [model,input] = case_reader(file_num)
% show = case_reader(file_num)
%
% when called with 2 output arguments, returns model and input, which are
% structures that contain everything model.m needs
% when called with 1 output argument, returns show (wheels and axes)

% check for correct number of arguments (1 or 2)
if nargout~=1 && nargout ~=2; error('something is horribly wrong'); end;

filename = ['cases/' num2str(file_num) '.txt'];

check = struct('wheels',0,'axes',0);
local.L = 0;

%% reads file only to find show- which wheels and axes to display
% show contains show.wheels and show.axes
if nargout == 1
        fid = fopen(filename);
        while ~feof(fid)
                key = textscan(fid,'%s',1,'delimiter',' ');
        value = textscan(fid,'%s',1,'delimiter','\n');
%         char(key{1,1}) % for testing
                switch char(key{1,1})
                        case 'wheels:'
                                if check.wheels; disp('wheels multiply defined'); end
                                show.wheels = str2num(cell2mat(value{:}));
                                check.wheels = 1;
                        case 'axes:'
                                if check.axes; disp('axes multiply defined'); end
                                show.axes = str2num(cell2mat(value{:}));
                                check.axes = 1;
                        otherwise
                                % do nothing
                end
    end
    fclose(fid);
        varargout(1) = {show};
    return
```

```
42 end
43
44 %% nargout must be 2-> read file for model configuration
45 %% set up geometry of wheels (#, orientation)
46 % orientation of spin axis (wheel z) in global coords
47 model.zps = [[0 0 1]' [0 0 1]' [0 0 -1]'];
48
49 % # wheels derived from zps
50 model.nwheels = size(model.zps,2);
51 %% set variables to defaults
52     model.busk = zeros(6); % no bus/support spring
53     model.dummy = 0; % no dummy mass (appendage)
54     % define dummy mass terms anyways, we'll just ignore them if dummy=0
55     model.mdummy = diag([1 1 1 10 10 1]);
56         kdummy = 1000*pi^2*diag([0 0 0 1 1 0]);%*1.23456;
57         model.kdummy = [-kdummy kdummy; kdummy -kdummy];
58
59     input.w = zeros(2,model.nwheels); % w = 0 for all wheels
60
61     % default is no initial input or state
62     qbuilder = zeros(12,(model.nwheels+model.dummy));
63     input.b = qbuilder;
64     input.b1 = qbuilder;
65
66     % default integration time
67     input.time = 1;
68
69     % empty ode45 options
70     model.options = [];
71
72 %% read the case file and set up the model
73 fid = fopen(filename);
74 while ~feof(fid)
75     key = textscan(fid,'%s',1,'delimiter',' \n');
76 %     char(key{:})
77     value = textscan(fid,'%s',1,'delimiter','\n');
78     value = cell2mat(value{:,:});
79     switch char(key{1,1})
80         case 'config:' % complete
81 %             value{1,1} for testing
82 %             config = value;
83             switch value
84                 case 'validation'
85                     [k,c,mwheel,msupport,L] = validation_model;
86                 case 'super'
87                     [k,c,mwheel,msupport,L] = super_model;
88                 case 'thesis'
89                     [k,c,mwheel,msupport,L] = super_model;
90                 case 'sub'
91                     [k,c,mwheel,msupport,L] = sub_model;
92                 otherwise; error('uh-oh')
93             end
94             model.k=k; model.c=c; model.mwheel=mwheel; ...
95                 model.msupport=msupport;
96 %             local =setfield(local,'L',L);
97             local.L = L;
98             local.config = value;
99         case 'busk' % complete
100             model.busk = -1e6*diag([0 0 0 1 1 0]);
101         case 'appendage' % complete
102             model.dummy = 1;
103         case 'time:' % complete
104             input.time = str2num(value);
105         case 'whz:' % complete
106             input.w = ones(2,3) .* str2num(value) * 2*pi;
107         case 'wrpm:' % complete
```

```
108             input.w = str2num(value) * 2*pi /60;
109         case 'damping:'  % complete
110 %             if str2num(cell2mat(value{:}))==0
111 %     str2num(value)
112             if str2num(value)==0
113                 local.c = 0;
114                 disp('damping is off')
115             else disp('i do not understand')
116             end
117         case 'input:' % complete
118             % this takes care of 'input.b' and 'input.b1'
119             eval(['input.' value ';']);
120         case 'state:' % complete
121             eval(value);
122         case 'options:' % complete
123             eval(['model.options.' value ';']);
124 
125         otherwise % return an error if something unexpected happens
126             test = char(key{1,1});
127             if isempty(test)
128             elseif strfind('wheels: axes: %',test)
129             else
130                 char(key{1,1})
131                 error('typo in input file');
132             end
133     end
134 end
135 fclose(fid);
136 try; cexist=local.c; end
137 % a = local.c
138 % c=c
139 % b = model.c
140 % adjust damping (usually to turn it off)
141 if exist('cexist','var'); model.c = model.c * local.c; end
142 
143 % build q0
144 input.q0 = qbuilder(:);
145 
146 fxy = 1; % this is unneccessary- all scaling is in e, so this is just 1
147 fab = fxy * local.L / 4;
148 
149 local.config
150 if strfind('thesis super sub ',local.config)
151     input.b(10:11,:) = input.b(10:11,:)*fab;
152     input.e = 1e-11 * model.mwheel(1,1); %
153 elseif strfind('validation',local.config)
154     input.e = 1;
155 end
156 
157 varargout(1) = {model};
158 varargout(2) = {input};
159 
160 return
161 
162     % imbalance scaling terms- may be used to create e later
163     % F_centripetal = mrw^2; e = mr; m = m_wheel; e = eccentricity
164     % this imbalance causes x/y vibe
165 
166     % this imbalance causes a/B vibe
167     % the model can't tell the difference, only scaling is in input.b
168     % from page 93 of notes
169 %
170 
171     % a/B imbalance input should just be 1, and i will here multiply it by
172     % fab
173 end
```

```
174
175 %% functions to set up common wheel properties for the 3 model types
176 function [k,c,mwheel,msupport,L] = validation_model
177         [k,msupport,L] = validation_model_params;
178         c = k/1000;
179         mwheel = validation_mass;
180 end
181 function [k,c,mwheel,msupport,L] = super_model
182         [k,msupport,L] = thesis_model_params;
183         c = k/500;
184         mwheel = super_mass;
185 end
186 function [k,c,mwheel,msupport,L] = sub_model
187         [k,msupport,L] = thesis_model_params;
188         c = k/500;
189         mwheel = sub_mass;
190 end
191 %% functions to create stiffness matrices
192 function [k,msupport,L] = validation_model_params
193     % distance from CG_support to CG_flywheel
194     d = 1;
195     L = 0.5;
196
197         k_mag = 2500; % (stiffness of each mag bearing)
198         kt = 2*k_mag; % linear transverse stiffness
199         kz = 0; % linear axial stiffness
200         Kt = k_mag*L^2/2; % angular- derived from k_mag
201         Kg = 0; % about flywheel rotation axis- zero
202         k_vector = [kt, kt, kz, Kt, Kt, Kg]' ;
203
204         k1 = -diag(k_vector)-diag([0 0 0 d^2*kt d^2*kt 0]); % upper left
205         a = [0 -d*kt; d*kt 0];
206         k1(1:2,4:5) = a;
207         k1(4:5,1:2) = a';
208         k2 = diag(k_vector);
209         k2(4:5,1:2) = a;
210         k3 = k2'; % lower left
211         k4 = -diag(k_vector); % lower right
212
213         k = [k1 k2; k3 k4];
214
215     % mass properties of support structure
216     mbus = 10;
217     I1 = 10;
218     I2 = 10;
219     I3 = 10;
220     msupport = diag([mbus,mbus,mbus,I1,I2,I3]);
221 end
222 function [k,msupport,L] = thesis_model_params
223     % distance from CG_support to CG_flywheel
224     d = .2;
225     L = .2;
226
227         % magnetic bearing stiffness
228         k_mag = 1756e3; % N/m (transverse stiffness of each mag bearing)
229         kz = 0; % linear axial stiffness- not modelled here
230         Kg = 0; % about flywheel rotation axis- zero
231
232         % model stiffnesses- derived from mag bearing stiffness
233         kt = 2*k_mag; % N/m (effective model stiffness- 2 bearings/flywheel)
234         Kt = k_mag*L^2/2; % N-m/rad (model angular stiffness- from k_mag)
235
236         % stiffness vector
237         k_vector = [kt, kt, kz, Kt, Kt, Kg]' ;
238
239         % turn my bearing stiffnesses into a stiffness matrix
```

```
240         k1 = -diag(k_vector)-diag([0 0 0 d^2*kt d^2*kt 0]); % upper left
241         a = [0 -d*kt; d*kt 0];
242         k1(1:2,4:5) = a;
243         k1(4:5,1:2) = a';
244         k2 = diag(k_vector);
245         k2(4:5,1:2) = a;
246         k3 = k2'; % lower left
247         k4 = -diag(k_vector); % lower right
248
249         k = [k1 k2; k3 k4];
250
251     % mass properties of support structure
252     mbus = 10; % kg
253     I1 = 10; % kg-m^2 (MOI about X)
254     I2 = 10; % (MOI about Y)
255     I3 = 10; % (MOI about Z)
256
257     msupport = diag([mbus,mbus,mbus,I1,I2,I3]);
258 end
259 %% functions to create mass matrices
260 function mwheel = validation_mass
261     m = 10;
262     L = 0.5;
263     r = 1/8;
264     It = m/12 * (3*r^2 + L^2);
265     Ip = m/2 * r^2;
266
267     mwheel = diag([m,m,m,It,It,Ip]);
268 end
269 function mwheel = super_mass
270     m = 10; % kg (mass of flywheel)
271     L = .2; % m (length of flywheel)
272     r = .15; % m (radius of flywheel)
273     It = m/12 * (3*r^2 + L^2); % kg-m^2 (transverse MOI)
274     Ip = m/2 * r^2; % (polar MOI)
275
276     % this is the number that is defined above
277     % It = 0.0896;
278
279     mwheel = diag([m,m,m,It,It,Ip]);
280 end
281 function mwheel = sub_mass
282     m = 10; % kg (mass of flywheel)
283     L = .2; % m (length of flywheel)
284     r = .15; % m (radius of flywheel)
285     It = m/12 * (3*r^2 + L^2); % kg-m^2 (transverse MOI)
286     Ip = m/2 * r^2; % (polar MOI)
287
288     % for demonstration of sub-sync whirl, redefine It- cases 72xx
289     It = 0.2015;
290
291     mwheel = diag([m,m,m,It,It,Ip]);
292 end
293
294
295
296
297 % model.options.MaxStep = 2e-4;
```

Listing B.3: ../models/crunch.m

```
1 function crunch(config,varargin)
2 global output
3
4 if nargin == 0; config = 'validate'; end;
5
```

```
if ~isnumeric(config)
    fid = fopen('case_maker.m');
    cases={};
    while ~feof(fid)
        garbage = textscan(fid,'%s',1,'delimiter','\n');
        cases = [cases; textscan(fid,'case %u',1)];
    end
    fclose(fid);
    cases = cell2mat(cases);
%     config = unique(b)';
    switch config
        case 'validate'
            config = cases(find(cases<1000));
        case 'test'
            config = cases(find(cases>=1000));
        case 'all'
            config = cases;
    end

end

%  return % for testing

% if length(config)>1; matlabpool open local; end;

% This code creates data for me if create_data by calling the model funct

parfor jj=1:length(config)
    ii = config(jj)
   [output] = model(ii);
   filename = strcat('data/', num2str(ii),'.mat');
   iSave(filename,output);
end

% if length(config)>1; matlabpool close; end;

fprintf('crunched!!!\r')


function iSave(filename,output)
filename
save(filename,'output')
```

Listing B.4: ../models/graph.m

```
function h = graph(config,show_plots,varargin)
h=[]; global output;

if nargin == 0; config='validate'; show_plots=0; end;

%% determine which cases to graph
if isnumeric(config)
    % if I only request 1 (or a few) plots- display them on screen
    if nargin==1||isempty(show_plots); show_plots = 1; end
else % read case_maker to see which plots to graph
    fid = fopen('case_maker.m');
    cases={};
    while ~feof(fid)
        garbage = textscan(fid,'%s',1,'delimiter','\n');
        cases = [cases; textscan(fid,'case %u',1)];
    end
    fclose(fid);
    cases = cell2mat(cases);
%     config = unique(b)';
    switch config
        case 'validate' % graph only my validation cases
```

```
            config = cases(find(cases<1000));
        case 'test' % graph only my test cases
            config = cases(find(cases>=1000));
        case 'all' % graph all cases found in case_maker
            config = cases;
    end
end

save_plots = 1;

%% crunch if necessary
crunch_this = [];
for ii = config
    filename = ['data/', num2str(ii), '.mat'];
    if ~exist(filename);
        crunch_this = [crunch_this ii];
    end;
end

if ~isempty(crunch_this); crunch(crunch_this); end

%% create graphs
for ii = config
    % load show.wheels and show.axes
    show = case_reader(ii);

    filename = ['data/', num2str(ii), '.mat'];
    load(filename)

    % Create graphs

    ncols = length(show.wheels);
    naxes = length(show.axes);

    label = {'$x ~\textrm{(m)}$','$y ~\textrm{(m)}$','$z ~\textrm{(m)}$',...
             '$\theta_x ~\textrm{(rad)}$','$\theta_y ~\textrm{(rad)}$',...
             '$\theta_z ~\textrm{(rad)}$',...
             '$\dot{x } ~\textrm{(m/s)}$','$\dot{y } ~\textrm{(m/s)}$',...
             '$\dot{z } ~\textrm{(m/s)}$',...
             '$\dot{\theta_x } ~\textrm{(rad/s)}$',...
             '$\dot{\theta_y } ~\textrm{(rad/s)}$',...
             '$\dot{\theta_z}~\textrm{(rad/s)}$'};

    figure(ii);
    set(gcf,'units','inches', 'position',[0 0 2.4*ncols 1.4*naxes],...
        'paperpositionmode',...
        'auto','papersize',[2.4*ncols-.5 1.4*naxes]);
    % this is pretty obfuscated to me- need some comments
    for c = 1:ncols % this cycles and creates naxes plots for each wheel
        wheel = show.wheels(c);

        for k = 1:naxes % this loop actually creates each plot
            axis = show.axes(k);
            h(k,c) = subplot(naxes,ncols,ncols*(k-1)+c);
            plot(output.t,output.q(:,axis+12*(wheel-1)));
            tf = output.t(length(output.t));
            set(gca,'xlim',[0 tf]);
                if c==1; ylabel(label{axis},'interpreter','latex'); end;
                if k==naxes; xlabel('time (s)'); end;

            % put correct wheel # label on only top subplot
            if k==1;
                % code's wheel #'s = reality + 1; (1 is bus)
                if wheel == 4
                    title('Appendage');
                elseif  wheel~=1;
```

```
                    title(['wheel ',num2str(wheel)-1]);
                else; title('Support');
                end
            end

        end

    end
%  save and/or show plots
    % create files of each plot
    if save_plots;
        % MATLAB fig file
        saveas(gcf,[fullpath('.\pics\figs'),'\case', ...
            num2str(ii)],'fig');
        % pdf file for inclusion in thesis
        saveas(gcf,[fullpath('./pics/pdfs'),'/case', ...
            num2str(ii)],'pdf');
        % png file for quick viewing of all cases- this one has case label
%         suplabel(['Case ', num2str(ii)],'t');
        saveas(gcf,[fullpath('./pics/pngs'),'/case', ...
            num2str(ii)],'png');
    end;
%     show_plots
    if ~show_plots; close; end;

end

fprintf('graphed!!!\r')
```

Listing B.5: ../models/spect_me.m

```
function spect_me(config,fmax,wheel,varargin)
% this will make spectrograms
global S F T P

if nargin < 3 ; wheel = 3; end

% done = [7210:7212  7222 ];%7310:7312]7221;
% if intersect(config,done);
%     error('already completed')
% end

%% create graphs
for jj = 1:length(config)
    ii = config(jj);

    filename = ['data/', num2str(ii), '.mat'];
    load(filename)

    %%
%     wheel = 1; % for testing
%     ii = 1; % for testing
%     fmax = 450; % for testing
    qnum = 12*(wheel-1)+4;

    x=output.q(:,qnum); % alpha of specified wheel (default 2)

    samples = length(output.t);
    time = output.t(samples);
    Fs = samples/time;

    segments = 30;
    poverlap = .95;
    window = floor(samples/segments);
    % nfft = max(2^nextpow2(window),2^12);
```

```
35      nfft = 2^15;
36      noverlap = floor(window * poverlap) ;
37
38  %     figure(1) % for testing
39      figure(ii+10000); clf;
40      set(gcf,'units','inches', 'position',[0 0 8 4],...
41          'paperpositionmode',...
42          'auto','papersize',[8 4]);
43      % S=spectrogram(x,window,noverlap,nfft,fs)
44      [S,F,T,P]=spectrogram(x,window,noverlap,nfft,Fs);
45
46      if nargin == 1;
47          fmax = 1000;
48      end;
49
50      Fmax = floor(fmax * 1000/F(1000));
51
52      % colorbar is messed up for signals <1e-20: so I multiply by 1e10
53      pcolor(T,F(1:Fmax),1e10*P(1:Fmax,:))
54  %     pcolor(T,F(1:Fmax),P(1:Fmax,:))
55      shading flat
56      colorbar
57      xlabel 'Time (s)'
58      ylabel 'Frequency (Hz)'
59
60  warning('Remember to manually edit the colorbar scale (it"s 1e10 too high)')
61
62      %%
63
64      %  save and/or show plots
65      % create files of each plot
66      % MATLAB fig file
67      saveas(gcf,[fullpath('.\pics\figs'),'\spec', num2str(ii)],'fig');
68  %     % pdf file for inclusion in thesis
69  %     saveas(gcf,[fullpath('./pics/pdfs'),'/spec', num2str(ii)],'pdf');
70      % png file for quick viewing of all cases- this one has case label
71  %     suplabel(['Case ', num2str(ii)],'t');
72      saveas(gcf,[fullpath('./pics/pngs'),'/spec', num2str(ii)],'png');
73
74
75  end
76
77  fprintf('spec''ed!!!\r')
78
79  end
```

Listing C.1: ../models/cases/sample.txt

```
% sample configuration file
% case = 730- this number is just a visual reference
% all comments must be behind %'s
% do not leave any blank rows
config: validation
busk
appendage
stiffness: 0
damping: 0
time: 10
whz: [[0;0] [4;12] [4;12]]
% or wrpm:
input: b(10:11,2:3) = 1e-3
wheels: 1 2 3
axes: 4 5
```

Listing C.2: ../models/cases/105.txt

```
config: validation
wheels: 1 2 3
axes: 1 2 4 5
time: 1
whz: 0
state: qbuilder(2,2:3) = 0.01
```

Listing C.3: ../models/cases/120.txt

```
config: validation
wheels: 2 3
axes: 4 10 5 11
time: 1
whz: 0
state: qbuilder(4,2:3) = 0.01*[1 -1]
state: qbuilder(11,2:3) = 0.4*[1 -1]
```

Listing C.4: ../models/cases/125.txt

```
config: validation
wheels:  2 3
axes:  4 10 5 11
busk
time: 1
whz: [[0;0] [10;10] -[10;10]]
state: qbuilder(4,2:3) = 0.01*[1 -1]
state: qbuilder(11,2:3) = 0.4*[1 -1]
```

Listing C.5: ../models/cases/126.txt

```
config: validation
wheels:  2 3
axes: 4 10 5 11
busk
time: 1
whz: [[0;0] -[10;10] [10;10]]
state: qbuilder(4,2:3) = 0.01*[1 -1]
state: qbuilder(11,2:3) = 0.4*[1 -1]
```

Listing C.6: ../models/cases/159.txt

```
config: validation
```

```
wheels: 1 2 3
axes: 1 2 4 5
whz: 0
time: 0.25
input: b1(10,1) = 0.01
options: MaxStep=2e-4
```

Listing C.7: ../models/cases/700.txt

```
config: thesis
wheels: 1 2 3
axes: 4 5
whz: [[0;0] [0;0] [5;5]]
input: b(10:11,3) = 100
time: 0.5
options: MaxStep=2e-4
```

Listing C.8: ../models/cases/701.txt

```
config: thesis
wheels: 1 2 3
axes: 4 5
whz: [[0;0] [5;5] [0;0]]
input: b(10:11,2) = 100
time: 0.5
options: MaxStep=2e-4
```

Listing C.9: ../models/cases/730.txt

```
% case = 730
% looking for critical coning speed at f_con ~~ 6.8 Hz
% use the validation model
% use the support spring
% input.e = 1;
config: validation
busk
wheels: 1 2 3
axes: 4 5
time: 10
whz: [[0;0] [4;12] [4;12]]
input: b(10:11,2:3) = 1e-3
```

Listing C.10: ../models/cases/4001.txt

```
config: thesis
wheels: 1 2 3
axes:  4 5
wrpm: [[0;0] [20;20] [20;60]]*1000
time: 10
input: b(7:8,3) = 1
options: MaxStep=2e-4
```

Listing C.11: ../models/cases/4002.txt

```
config: thesis
wheels: 1 2 3
axes:  4 5
wrpm: [[0;0] [60;60] [20;60]]*1000
time: 10
input: b(7:8,3) = 1
options: MaxStep=2e-4
```

Listing C.12: ../models/cases/4003.txt

```
config: thesis
wheels: 1 2 3
axes:  4 5
wrpm: [[0;0] [60;20] [20;60]]*1000
time: 10
input: b(7:8,3) = 1
options: MaxStep=2e-4
```

Listing C.13: ../models/cases/6012.txt

```
config: thesis
wheels: 1 2 3
busk
axes:  4 5
whz: [[0;0] 3000/9*[1;1] (3000/9+5)*[1;1]]
time: 1
input: b(10:11,2:3) = 1
options: MaxStep=2e-4
```

Listing C.14: ../models/cases/6013.txt

```
config: thesis
wheels: 1 2 3
axes:  4 5
busk
whz: [[0;0] 3000/9*[1;1] 0*[1;1]]
time: 1
input: b(10:11,2:3) = 1
options: MaxStep=2e-4
```

Listing C.15: ../models/cases/6017.txt

```
config: thesis
appendage
busk
wheels: 1 2 3 4
axes:  4 5
whz: [[0;0] 3000/9*[1;1] (3000/9+5)*[1;1]]
time: 1
input: b(10:11,2:3) = 1
options: MaxStep=2e-4
```

Listing C.16: ../models/cases/6018.txt

```
config: thesis
appendage
busk
wheels: 1 2 3 4
axes:   4 5
whz: [[0;0] 3000/9*[1;1] 400*[1;1]]
time: 1
input: b(10:11,2:3) = 1
options: MaxStep=2e-4
```

Bibliography

1. Bedford, Anthony and Wallace Fowler. *Engineering Mechanics: Dynamics*. Prentice Hall, 2002.

2. Delventhal, Rex A. "Flywheel Energy Storage System Designed for the International Space Station". *Research and Technology 2001*, 204–205. NASA Glenn Research Center, 2002. URL `www.grc.nasa.gov/WWW/RT/RT2001/index.html`. NASA/TM–2002-211333.

3. Doyle, Michael R., Douglas J. Samuel, Thomas Conway, and Robert R. Klimowski. "Electromagnetic Aircraft Launch System - EMALS". URL `www.navair.navy.mil/lakehurst/nlweb/ieeerevc.pdf`. Retrieved 22 Jan 11.

4. Duffy, Kirsten P. "RE: flywheels", Feb 2011. E-mail.

5. Genta, Giancarlo. *Kinetic energy storage: theory and practice of advanced flywheel systems*. Butterworths, 1985.

6. Hall, Christopher D. "High Speed Flywheels for Integrated Energy Storage and Attitude Control". *Proceedings of the American Control Conference*. Jun 1997.

7. Hall, Christopher D. *Integrated Spacecraft Power and Attitude Control Systems Using Flywheels*. Technical Report AFIT/ENY/TR-000, AFIT, Oct 2001. URL `http://www.aoe.vt.edu/~cdhall/courses/aoe4065/litrev.pdf`.

8. Hibbeler, R. C. *Engineering Mechanics: Statics*. Pearson Prentice Hall, eleventh edition, 2007.

9. Jansen, Ralph H. "G2 Flywheel Module Operated at 41,000 rpm". *Research & Technology 2004*, 132–133. NASA Glenn Research Center, 2005. URL `www.grc.nasa.gov/WWW/RT/2004/RS/RS10S-jansen.html`. NASA/TM–2005-213419.

10. Jansen, Ralph H. "Integrated Power and Attitude Control System Demonstrated With Flywheels G2 and D1". *Research & Technology 2004*, 95–96. NASA Glenn Research Center, 2005. URL `www.grc.nasa.gov/WWW/RT/2004/RS/RS10S-jansen.html`. NASA/TM–2005-213419.

11. Jansen, Ralph H., Ramon Lebron, Timothy P. Dever, and Arthur G Birchenough. "PWM SWITCHING FREQUENCY EFFECTS ON EDDY CURRENT SENSORS FOR MAGNETICALLY SUSPENDED FLYWHEEL SYSTEMS". *Proceedings of the 1st International Envergy Conversion Engineering Conference*. American Institute of Aeronautics and Astronautics, Inc., Aug 2003.

12. Lappas, V., D. Richie, C. Hall, J. Fausz, and B. Wilson. "Survey of Technology Developments in Flywheel Attitude Control and Energy Storage Systems". *Journal of Guidance, Control, and Dynamics*, 32(2), Mar–Apr 2009.

13. Lau, Jimmy, Sanjay S. Joshi, Brij N. Agrawal, and Jong-Woo Kim. "Investigation of Periodic-Disturbance Identification and Rejection in Spacecraft". *Journal of Guidance, Control, and Dynamics*, 29(4):792–798, Jul–Aug 2006.

14. McLallin, Kerry L., Ralph H. Jansen, Jerry Fausz, and Robert D. Bauer. "Aerospace Flywheel Technology Development for IPACS Applications". *36th Intersociety Energy Conversion Engineering Conference*. 2001.

15. Park, Junyoung. *MIMO Active Vibration Control of Magnetically Suspended Flywheels for Satellite IPAC Service*. Ph.D. thesis, Texas A&M University, May 2008.

16. Rao, Singiresu S. *Vibration of Continuous Systems*. John Wiley & Sons, 2007.

17. Reid, J. Gary. *Linear System Fundamentals*. McGraw-Hill, Inc., New York, 1983.

18. Slater, Joseph C. "Vibration Testing, With Modal Analysis and Health Monitoring", 2002. Unpublished text.

19. Soeder, James F. "Flywheel Single-Axis Integrated Momentum and Power Control System Demonstrated". *Research & Technology 2003*, 64–65. NASA Glenn Research Center, 2004. URL `http://www.grc.nasa.gov/WWW/RT/2003/5000/5450soeder.html`. NASA/TM–2004-212729.

20. Stanton, Bill, Joe Saliba, Craig Driscoll, and Dave Eisenhaure. "Aerospace technology making its way into terrestrial applications". *AIAA 34th Aerospace Sciences Meeting and Exhibit*. Jan 1996.

21. Vance, John, Fouad Zeidan, and Brian Murphy. *Machinery Vibration and Rotordynamics*. John Wiley & Sons, 2010.

22. Vance, John M. *Rotordynamics of Turbomachinery*. John Wiley & Sons, Inc., New York, 1988.

Vita

Jordan Firth graduated from the U.S. Air Force Academy in 2006 with a Bachelor's degree in Engineering Mechanics. After an assignment to Holloman AFB, New Mexico, where he worked as a test engineer at both the 586 Flight Test Squadron (meep meep) and the 846 Test Squadron (Holloman High Speed Test Track), he was sent to Wright-Patterson AFB, Ohio to get a Master's degree in Astronautical Engineering from AFIT. After graduation, he will be assigned to Los Angeles AFB, California to work on SBIRS.

REPORT DOCUMENTATION PAGE

Form Approved
OMB No. 0704-0188

1. REPORT DATE *(DD-MM-YYYY)*	2. REPORT TYPE	3. DATES COVERED *(From - To)*
24-03-2011	Master's Thesis	Aug 2009 - Mar 2011

4. TITLE AND SUBTITLE
Vibration Interaction in a Multiple Flywheel System

5a. CONTRACT NUMBER

5b. GRANT NUMBER

5c. PROGRAM ELEMENT NUMBER

6. AUTHOR(S)
Firth, Jordan A., Capt, USAF

5d. PROJECT NUMBER

5e. TASK NUMBER

5f. WORK UNIT NUMBER

7. PERFORMING ORGANIZATION NAME(S) AND ADDRESS(ES)
Air Force Institute of Technology
Graduate School of Engineering Management (AFIT/EN)
2950 Hobson Way
WPAFB OH 45433-7765

8. PERFORMING ORGANIZATION REPORT NUMBER
AFIT/GA/ENY/11-M03

9. SPONSORING/MONITORING AGENCY NAME(S) AND ADDRESS(ES)
National Aeronautics and Space Administration Glenn Research Center
Ray Beach, raymond.f.beach@grc.nasa.gov, (216) 433-53203
Mail Stop 301-5
21000 Brookpark Rd
Cleveland OH 44135

10. SPONSOR/MONITOR'S ACRONYM(S)
NASA GRC

11. SPONSOR/MONITOR'S REPORT NUMBER(S)

12. DISTRIBUTION/AVAILABILITY STATEMENT
APPROVED FOR PUBLIC RELEASE; DISTRIBUTION UNLIMITED

13. SUPPLEMENTARY NOTES
This material is declared a work of the U.S. Government and is not subjet to copyright protection in the United States

14. ABSTRACT

This study uses a linear model of an Integrated Power and Attitude Control System (IPACS) to investigate the vibration interaction between multiple flywheels. An easily extendable Matlab® script is created for the analysis of flywheel vibrations. This script is used to build a vibration model consisting of two active magnetic bearing flywheels mounted on a support structure. The flywheels are rotated at varying speeds, with an imbalance-induced centripetal force in one or both wheels causing vibrations in both wheels. Flywheel and system responses are examined for low frequency vibrations which would cause undesirable excitation to a satellite using IPACS, with a specific focus on the beat phenomenon and extra-synchronous vibration. Extra-synchronous resonant vibration between multiple rotors is shown to exist in an ideal undamped configuration but even a very small realistic amount of damping is enough to mitigate the effect enough that it is of less concern than individual rotor vibration inputs. Extra-synchronous resonant vibration is thus shown to have a minimal effect on satellite IPACS operation.

15. SUBJECT TERMS
flywheel, IPACS, gyroscope, satellite vibration

16. SECURITY CLASSIFICATION OF:			17. LIMITATION OF ABSTRACT	18. NUMBER OF PAGES	19a. NAME OF RESPONSIBLE PERSON
a. REPORT	b. ABSTRACT	c. THIS PAGE			Jonathan T. Black (ENY)
U	U	U	UU	110	19b. TELEPHONE NUMBER *(Include area code)* (937) 255-3636 x8991 jonathan.black@afit.edu